The International Journal of Advanced Manufacturing Technology (2019) 100:637–661
https://doi.org/10.1007/s00170-018-2726-y

ORIGINAL ARTICLE

Micro machining of bulk metallic glasses: a review

Lin Zhang [1,2] · Hu Huang [1]

Received: 10 March 2018 / Accepted: 17 September 2018 / Published online: 27 September 2018

Abstract
Bulk metallic glasses (BMGs) formed by rapid quench from liquid melts are emerging as a novel class of versatile advanced materials with excellent mechanical, physical, and chemical properties over conventional crystalline metals, including superior strength, high elasticity, and excellent corrosion resistance, attributable to their long-range disordered atomic structure. For practical applications, shaping of BMGs is the first process and various processing methods have been proposed. Apart from thermoplastic forming (TPF), micro machining processes, such as diamond turning, laser processing, and micro electrical discharge machining (micro-EDM), belonging to material removal processes, play significant roles for shaping of BMGs in industrial applications. In this review, the state-of-the-art micro machining methods of BMGs are comprehensively summarized, followed by pointing out future developments of this research topic. The reported studies are categorized into three different machining processes, termed as diamond turning, laser processing, and micro-EDM. Due to excellent properties of BMGs as well as amorphous structures, some unique cutting characteristics on the aspects of chip formation, cutting forces, tool wear, oxidization, and crystallization are reported during diamond turning process of BMGs. As the low machining efficiency and severe tool wear impede its broad commercial adoption, laser processing and micro-EDM exert their advantages on micro machining of BMGs. In consideration of the effects of laser irradiation on the multi-component alloys, understanding the fundamental laser-BMG interaction is necessary for the improvement and optimization of the machining precision and accuracy. Micro-EDM, as a novel kind of feasible processing method, further enlarges the machinability of BMGs. Some related issues and challenges in micro-EDM are carefully discussed, which are meaningful for further development of such method in micro/nano machining of BMGs.

Keywords Bulk metallic glasses · Diamond turning · Laser processing · Micro electrical discharge machining

1 Introduction

Bulk metallic glasses (BMGs) are a novel class of metallic alloys, formed by rapid quench from multi-component liquid melt. The absence of crystalline atomic structures endures them with some extraordinary mechanical, physical, and chemical properties over conventional metals [1]. In 1960, the metallic glass was firstly synthesized and reported by Klement et al. at California Institute of Technology [2]. The discovery was further developed by Chen et al. in 1970s [3]. As an important milestone in this field, he obtained a series of Pd-T-P amorphous arrays (T = Ni, Co, Fe) with critical casting thickness [4]. These new materials possess long-range disordered atomic structure with multiple components, which are similar to that of transparent glass. After that, more achievements were made in 1980s and a variety of BMG systems with high glass-forming ability were developed, such as Zr- [3, 5–8], Ti- [9, 10], Cu- [11, 12], Fe- [13–15], Mg- [16–18], Ni- [19, 20], and Pd- [21–23] based systems, as shown in Fig. 1. Compared with their crystalline counterparts, the cooling rates of the metallic elements in liquid phase are hundreds or thousands of times larger, quicker than a specified critical cooling rate. The transition time and buffer time between the liquid and solid phase are so short that is not enough for free atoms inside it to organize themselves into the ordered metallic lattice positions, remaining in the metastable state in solid. Because of the absence of grain boundary and

✉ Hu Huang
huanghu@jlu.edu.cn

[1] School of Mechanical Science and Engineering, Jilin University, Changchun 130022, Jilin, China

[2] Department of Integrated Systems Engineering, The Ohio State University, Columbus, OH 43210, USA

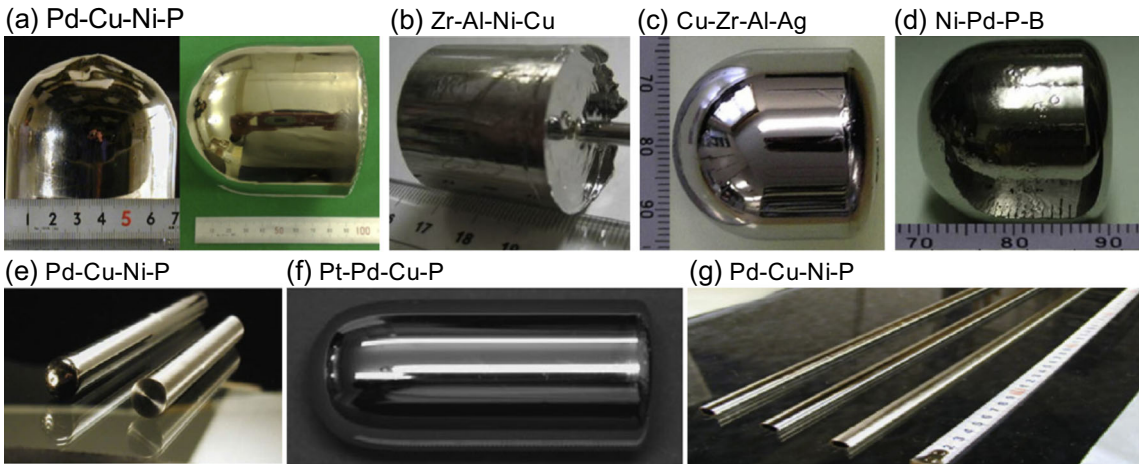

Fig. 1 Pd-, Ni-, Cu-, and Zr-based BMGs with centimeter size [26]

dislocation defect, BMGs present some outstanding properties, such as superior strength, high elasticity, and excellent corrosion resistance [24]. These attractive properties make them to be promising advanced structural and functional materials in the future, and extensive research and works have been done to explore new BMGs with stronger mechanical properties [24–26].

Right now, various BMGs with multiple components have been developed with different dimensions from several millimeters to tens of centimeters [27], and some of them have been selected as ideal candidates for many industrial and civil applications [4], for example structural material, sensor, spring, sporting goods, wear-/corrosion-resistant coating, optical, magnetic, micro-/nano-technology, information data storage, ornamental, biomedical, and fuel-cell separator materials [26].

Due to their special amorphous atomic structure, the plastic deformation and mechanism of BMGs are related to shear banding, being significantly different from the conventional crystalline metals, which are based on dislocation propagation and grain boundary subjected to external loads [28]. As no crystalline defect and grain boundary exist, BMGs are ideal materials for applications in micro-/nano-devices. For practical applications, shaping of BMGs is the first and the most important process before any applications. The amorphous atomic structure within the supercooled liquid region endures them with an easy alternative shaping method at elevated temperature [29], i.e., thermoplastic forming (TPF). TPF provides a remarkable, near net-shaping and low-cost method for manufacturing large-scale, precise, and versatile geometries on electrical, biomedical, and optical elements [4], as shown in Fig. 2. However, TPF requires ultra-precision molds, which are quite difficult to fabricate but very easy to damage especially when the micro/nano structures on the mold is complex. Moreover, TPF can only copy simple structures on the mold which is not flexible for complex three-dimensional (3D) or customer-designed applications. Therefore, alternative methods for shaping BMGs should be further explored and developed.

Diamond turning, assisted with fast/slow tool servo (F-/STS), has been widely accepted as a very promising technology for flexible ultra-precision machining of freeform surface [30–35]. Due to its superior advantages of generating high profile accuracy and optical finish surface, it has been generally employed to fabricate complicated, periodic, or functional microstructures on biomedical and optical elements [30, 36–38], such as hydrophobic/hydrophilic surface [39]. As one of the most basic methods in mechanical machining, intensive investigations on the machining of BMGs have been conducted in the past decades, including the separation mechanism between the BMG surface and the chips [37, 40, 41], diamond tool graphitization and wear [42], finished surface roughness [43], and so on.

Micro machining of BMGs with high-power laser system, as a typical non-contact material removal method, also presents interesting fabrication opportunities due to the inherent high-throughput of such approach and its associated ability for processing a broad range of materials regardless of their mechanical properties [44]. At the same time, recent development in laser micro machining has achieved great interest for their applications in fabricating micro structures [45–48]. Because laser processing will ultimately produce heating and cooling cycles within the materials, the cycles should be limited within a short range whereby the machining process will not introduce crystallization precipitates into the microstructure of the materials [49, 50]. Therefore, many efforts were conducted to investigate the interaction between a pulsed/continuous laser beam and BMGs for further generating surface structures with micro-scale dimensions [51].

Micro electrical discharge machining (micro-EDM), as another kind of non-contact machining method, becomes one popular machining method for micro machining of BMGs. Compared with diamond turning and laser processing, micro-EDM is a more flexible production method for

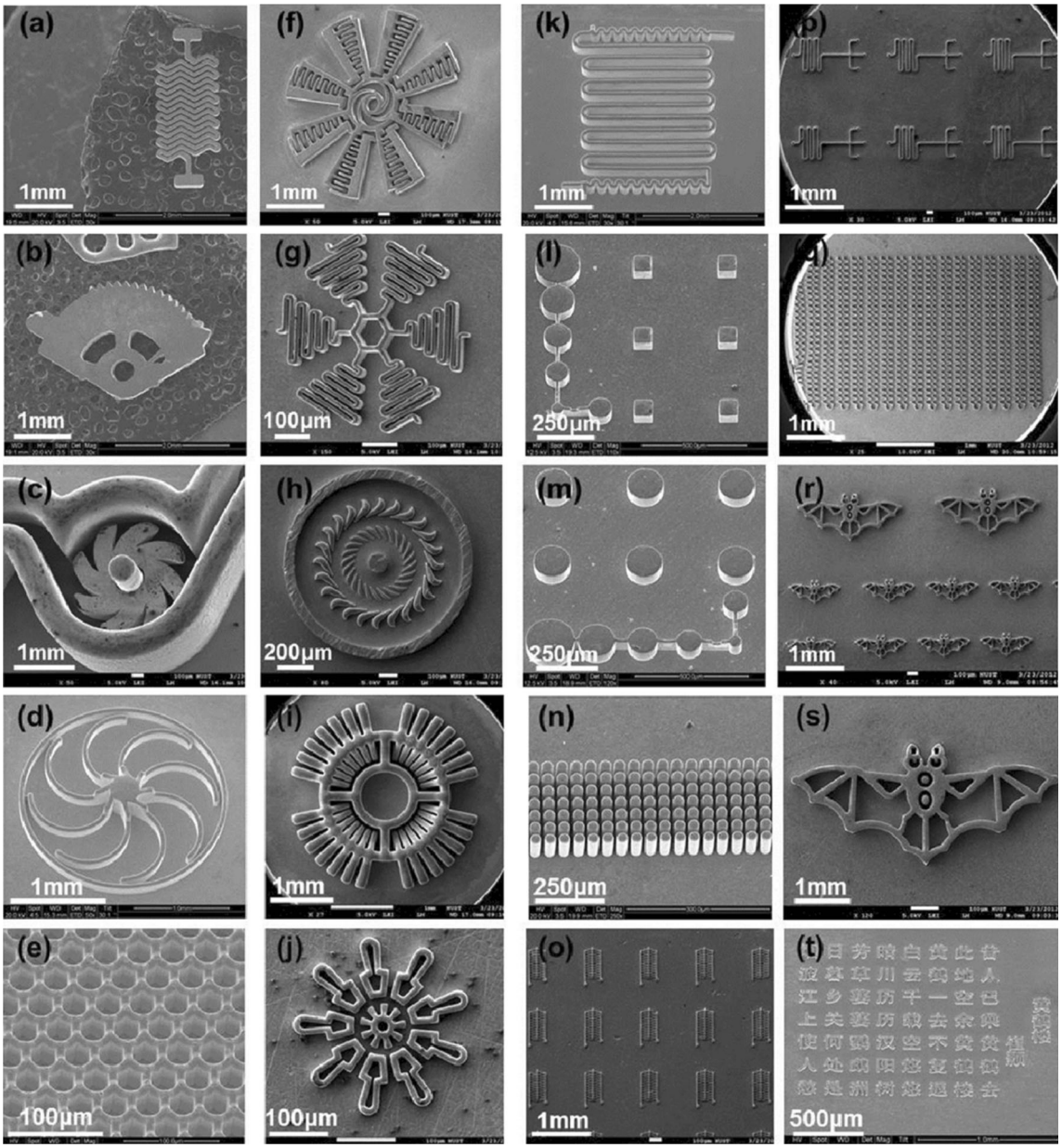

Fig. 2 Typical thermoplastic forming devices with micro-/nano-patterns for MEMS application: **a**–**g** micro-spring, micro-gear, micro-motor, micro-fan, micro-honeycomb structure, micro-gyroscope, and micro-accelerometer structure; **h**–**j** micro-tubines; **k**–**q** patterns used in biochips; and **r**–**t** fancy surface patterns such as micro-bats and micro-poetry [4]

fabricating 3D micro-parts with sub-micro structures, such as micro-hole, micro-gear, micro-array, and micro-tool [52–54]. In addition, micro-EDM is also suitable for machining hard-brittle materials which is quite difficult by conventional machining methods, such as diamond turning and high-speed micro milling. Therefore, it has been widely employed in die and mold making industry. In consideration of the outstanding mechanical properties of BMGs especially the high hardness, micro-EDM becomes a potential choice for machining some hard-brittle BMGs. However, micro-EDM is an electro-thermal process and BMGs are very sensitive to temperature. Some results obtained by Hsieh et al. [55] indicated that severe crystallization happened during the conventional EDM of Zr-based BMG because of high electrical discharge energy leading to concentrated local heat. The microstructural changes of BMGs in deeper subsurface region, i.e., heat-affected zone, have not been clearly clarified.

In the past decade, a few reviews have been published on different and specific aspects of BMGs related to the synthesis, properties, and applications by Axinte [56], Lu and Liu [57], Schroers [1], et al. Axinte gave a general view of the development and recent advance of BMGs on material properties and applications [56]. Schroers presented a detailed review on the processing of BMGs, including the casting,

thermoplastic forming, and their effects on the material properties [1]. Most of previous reviews are focused on the thermoplastic forming process of BMGs. However, micro machining by material removal approaches has been rapidly developed and made great achievements in recent years. These machining methods undoubtedly play very important roles in BMG micro machining, especially for precision micro-/nano machining. Up to now, progresses related to such machining methods have not been systematically reviewed.

Toward an in-depth understanding of the issues in micro machining of BMGs, this review aims to present the recent developments and achievements on micro machining of BMGs, as well as some issues and challenges. As three important micro machining methods for BMGs, diamond turning, laser processing and micro-EDM, are emphasized to be discussed. Both the current and new potential applications, as well as issues and challenges are highlighted. Finally, we briefly summarize the progress of these three BMG micro machining methods and present the wide range of applications in future, including the potential capabilities for a number of industrial and biomedical relevant processes.

2 Diamond turning of BMGs

2.1 Introduction to diamond turning

Diamond turning is a cutting process using diamond tools. It belongs to one of the most widely used material removal methods by mechanical interactions between natural or synthetic diamond-tipped tool bits and workpieces. It has been widely employed to fabricate high-quality complex optics elements from crystals, metals, acrylic, and other materials by the contacting radiused tool noses [58]. Diamond turned surface has high specular surface quality and requires no additional polishing or buffing, unlike other conventionally machined surfaces.

Figure 3 illustrates the hardware configuration and working principle of the machining process. The computer numerical control (CNC) machine tool is composed of two main components, namely a spindle to install and rotate the workpiece and a multi-axis linear stages moving in the x-axis, y-axis, and z-axis. Generally, the y-axis is not activated during diamond turning process. The FTS utilized on the turret serving as an auxiliary moving axis is specially adopted to activate the diamond tool in and out of the workpiece when the spindle is rotating as programming [30]. For the diamond turning system, the geometry of the desired surface is usually expressed in cylindrical coordinates o_w-$x_w y_w z_w$, as shown in Fig. 3b. The function of the desired surface in the cylindrical coordinates can be presented as $z = f(\rho, \varphi)$, and the interval between two points on the spiral curve is determined by constant angle/distance sampling strategy.

For processing BMGs, diamond turning is particular useful. This is due to the fact that the diamond turning is one kind of micro machining methods without introducing significant thermal effect [30], which means BMGs could remain amorphous structure and avoid oxidization during diamond turning. When utilizing diamond turning for micro machining of BMGs, it is a complex interaction between the diamond tool and BMGs, accompanied by friction, deformation, and thermal conduction. The rapid heating and cooling rates associated with diamond turning can aid in then avoidance of crystallization, which allows the thermal effect zone retain its desirable properties after machining [59, 60]. The finish surface quality is not only dependent on the surface roughness, but also the resulting surface atomic structure after friction and deformation with diamond tool. Due to the absence of grain boundary and dislocation defect, the conventional deformation principle, fit for crystalline metals, does not match that for BMGs anymore, and the tool suffers seriously in such processing. Therefore, understanding the fundamental mechanism in micro machining between the diamond tool and BMG becomes critical for improving the surface quality, extending tool life, and increasing machining efficiency.

2.2 Investigation on chip formation and tool wear

The investigation on chip formation has been a long-standing subject in metal machining. For conventional crystalline alloys, substantial progress has been achieved for understanding the mechanism of diamond turning. However, as BMGs are a relative young group of alloy materials, the understanding of the deformation behavior and its underlying physics in BMG cutting processes lags is far from complete. The mechanism of chip formation is of central importance in diamond turning.

Previous studies presented that unique continuous chips with lamellar structure were prone to form during micro machining of BMGs. Using a TiN-coated WC-Co insert (Seco CCMT 09T304) with a 0.4-mm tip radius and a 5° rake angle, Bakkal et al. [41] investigated the effect of varying the cutting speed from 0.38 to 1.52 $m{\cdot}s^{-1}$ on the $Zr_{52.5}Ti_5Cu_{17.9}Ni_{14.6}Al_{10}$ BMG block. After machining, the chips were characterized by scanning electron microscope (SEM). It was observed that large shear lamella occurred with low cutting speed as shown in Fig. 4a, b, somewhat similar to the serrated chips produced in the turning process of Ti alloys [61–66]. Void formation occurred in the shear zone between lamella without consistent chip twist or curl. At high cutting speed, chip formation was a combination of irregular lamellar segments in the midsection, as shown in Fig. 4c. The presence of extensive viscous flow in the chips modified or inhibited a free-volume shear mechanism as in slow speed machining.

A study by Jiang et al. [67] provided further understanding regarding the structure evolution of Vit 1 BMG subjected to diamond turning. By observing the chips with high-

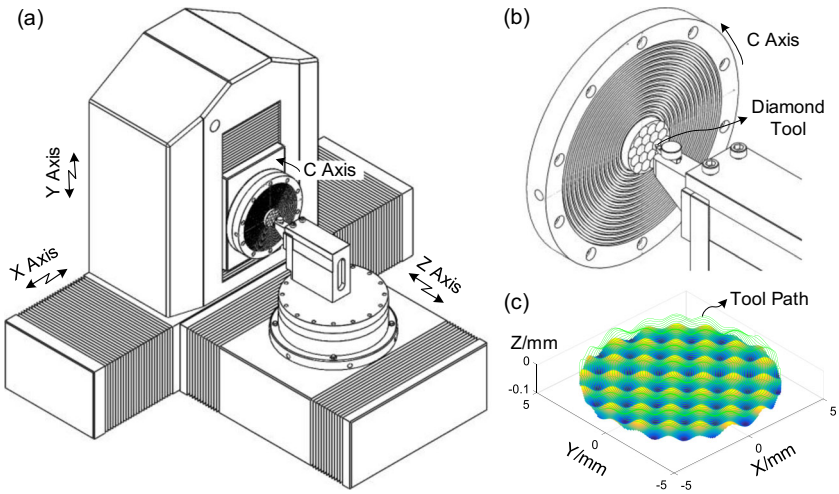

Fig. 3 Schematic diagrams of **a** diamond turning on a multi-axis ultra-precision lathe, **b** relative positions of the workpiece and diamond tool, and **c** microstructured surface and the tool path above the reference plane

magnification micrograph, periodic micro/nano structures with constant spacing in micrometer scale were achieved, as shown in Fig. 5. Furthermore, a coupled thermo-mechanical orthogonal cutting model, taking into account force, free volume, and energy balance in the primary shear zone (PSZ), was developed to quantitatively characterize the lamellar chip formation. The symmetry breaking of free volume flow and source governs the onset of lamellar chips, while the thermal instability only affects their morphology at low cutting speed.

The roughness of the machined surface was further studied by Bakkal et al. [42]. The averaged R_a of machined surfaces was summarized in Table 1. Compared with the machined surface by using WC-CVD, higher R_a was achieved by using WC-PVD and PCD tools that generated serrated BMG chips. The deteriorated surface roughness for WC-PVD and PCD tools may result from the generation of dynamic motion at the tool tip due to the formation of the periodical shear bands. Regular lathe turned surfaces with groove marks were observed on the machined BMG surface as shown in Fig. 6a. Furthermore, the roughness of the machined BMG surfaces was generally better than those of the machined Al6061 and SS304 surfaces, indicating that diamond turning is a potential method to obtain very precise BMG surface for optical and photonic applications.

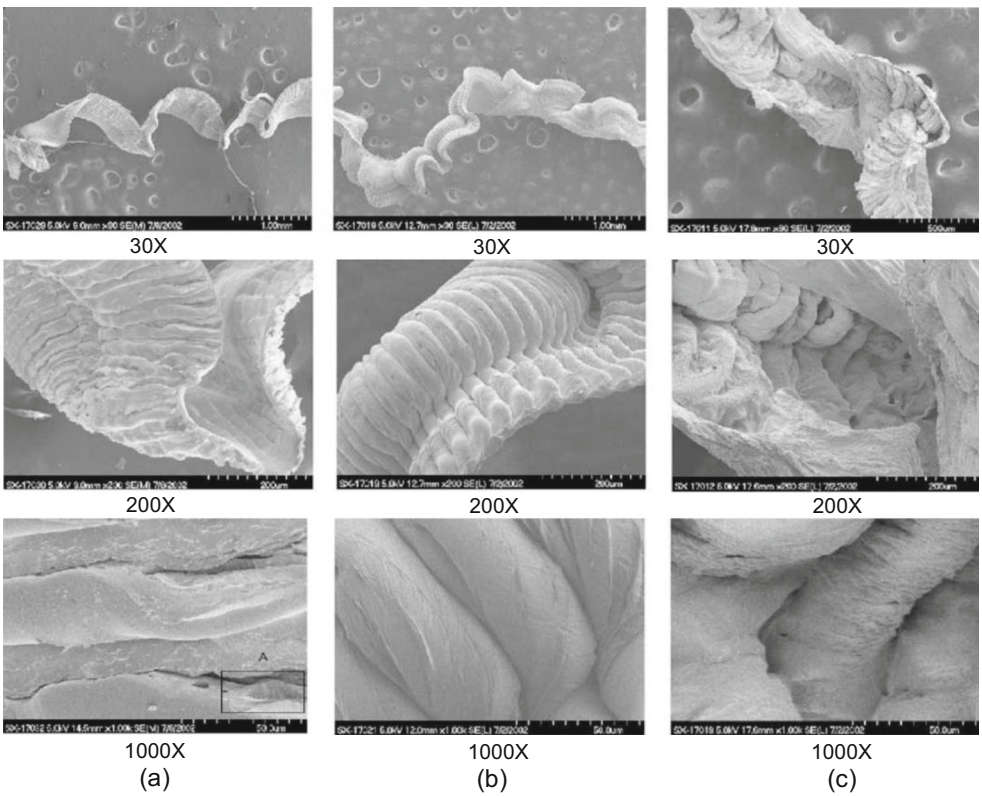

Fig. 4 SEM micrographs of chips at different magnification scales. Cutting speeds: **a** 0.38 m·s^{-1}, **b** 0.76 m·s^{-1}, and **c** 1.52 m·s^{-1} [41]

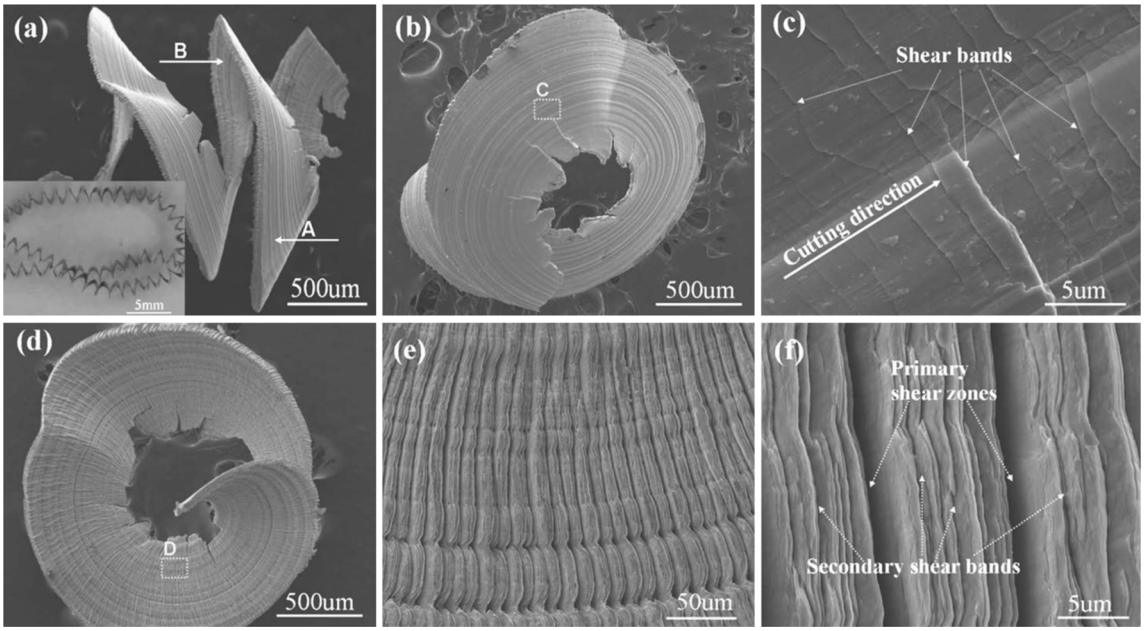

Fig. 5 Chip morphologies of Vit 1 BMG. **a** Macroscopic full-view of "continuous" twist chip; **b** tool–contact surface of chip marked by "A" in **a**; **c** details corresponding to area "C" in **b**; **d** free surface of chip marked by "B" in **a**; **e**, **f** lamellar structures at different magnifications in area "D" in **d** [67]

Due to the excellent mechanical properties of BMGs, an extensive study of tool wear was important for efficient and precision micro machining. The SEM micrograph of polycrystalline cubic boron nitride (PCBN) tool after machining of BMG is presented in Fig. 7. Because of the poor thermal conductivity of BMGs, the cutting heat was trapped in the workpiece-tool tiny local zone, promoting the welding of the chip to the tool tip. In Fig. 7, around the tool nose radius region where most of the cutting action occurred, it was observed that the chipping at cutting edge appeared. Moreover, along the cutting edge adjacent to the tool tip, the chipping also occurred although the physical contact between the tool and the workpiece did not occur in this area. Accordingly, it was derived that the impact of BMG chip with the tool edge during machining resulted in the occurrence of chipping [42].

2.3 Oxidation and crystallization

Another focused phenomenon in diamond turning, reported by Bakkal et al. [68], was the oxidization and crystallization of BMGs at high-speed diamond turning. The relevant properties of BMGs to this issue are the very low thermal conductivity and sensitivity to temperature variation during processing [68]. The cutting heat generated due to the interaction between the workpiece and tool was trapped in the narrow primary shear zone. Thus, high temperature could appear during diamond turning of BMGs, which may initiate the crystallization and oxidation of BMGs. As illustrated in Fig. 8, optical micrographs of polished cross-sections of the BMG chips machined at two cutting speeds of 0.38 and 1.52 $m{\cdot}s^{-1}$ showed different structures in different grayscale regions. In Fig. 8b, a dark oxide layer was visible around the chips and associated with the light emission during machining at 1.52 $m{\cdot}s^{-1}$ cutting speed, while no such oxide layer was observed in the chips at 0.38 $m{\cdot}s^{-1}$ cutting speed, as shown in Fig. 8a. Further observation was conducted after the BMG chip was polished and etched. Figure 9 shows various micro structural regions in these machined chip cross-sections. Chemical etching revealed the oxide layer on the outside surface of the chip and the dendritic pattern inside the chip. The dendritic pattern was due to crystallization of the BMG. Figure 9a, b shows the homogenous crystallization inside the chip, and Fig. 9c, d presents some dendritic patterns in the chips, which may match the direction of maximum cooling rate during the chip cooling. X-ray diffraction (XRD) was also performed on both the chips and machined surfaces to verify the oxidization and crystallization, as shown in Fig. 10.

To further understand the chip crystallization, the BMG chips obtained at 1.52 $m{\cdot}s^{-1}$ was investigated by using the field-emission SEM (FESEM) [68]. Figure 11 shows the region with mixed crystalline and amorphous structure under different gray levels and magnifications. Four regions with

Table 1 Average arithmetic surface roughness R_a (μm) [42]

Tool materials	WC-CVD	WC-PVD	PCD
BMG	0.47	0.84	0.62
Al6061	1.17	0.85	1.07
SS304	2.71	2.53	1.50

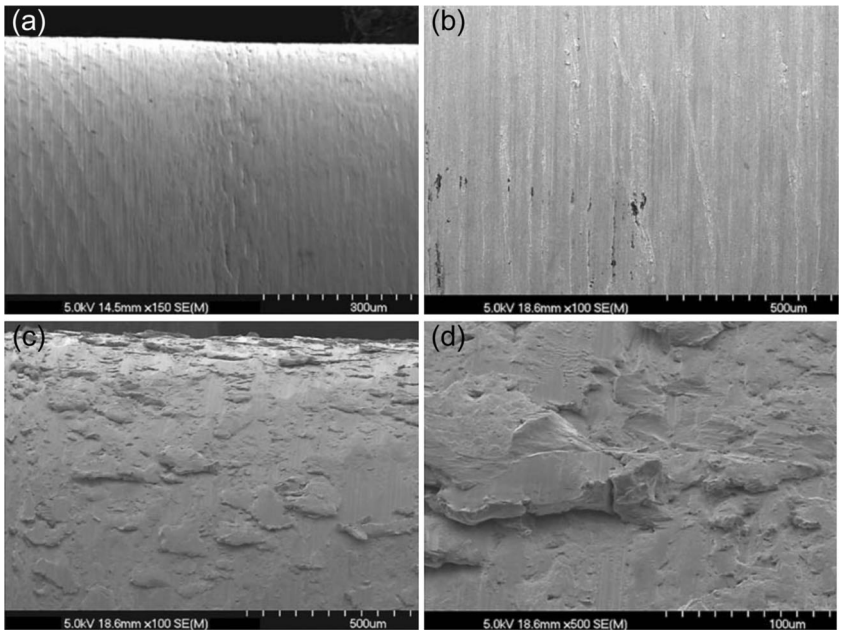

Fig. 6 SEM micrographs of the machined surfaces at 0.76 m·s^{-1} cutting speed. **a** BMG; **b** A16061; **c** SS304; and **d** SS304 (close-up view) [42]

different structures can be identified, oxide layer (O), crystalline phase (G), amorphous region (A), and eutectic region (E). The whole chip was surrounded by the oxide layer, while the eutectic region was mixed inside the amorphous region of the chips, and most of the leaf-shape crystalline phases, with dark gray color were distributed among the eutectic region.

Further works were done with different tool rake angles, coatings, and tool thermal conductivities [42]. The experimental results suggested that the high rake angle resulted in lower cutting force, and less thermal effect on the chip. No chip oxidation and light emission was observed in BMG micro machining by high rake angle tool (WC-PVD), resulted from different material deformation mechanisms, as shown in Fig. 12. Furthermore, different tool materials were adopted for turning experiments. If the tool had a high thermal conductivity, more heat could be conducted to the tool at the tool-chip interface. Thus, the chip temperature could be reduced, suppressing the chip oxidation and light emission during turning of BMGs.

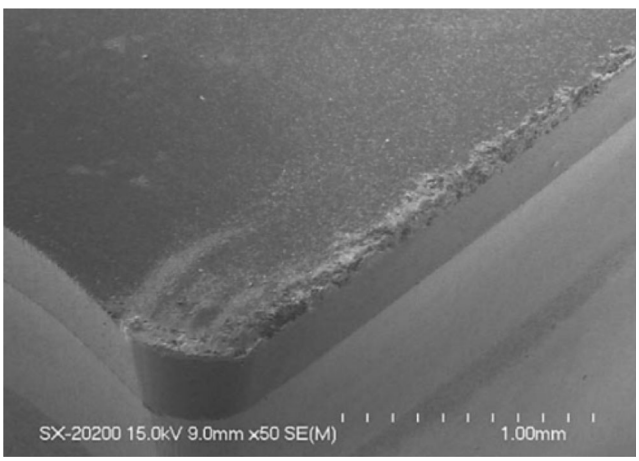

Fig. 7 PCBN tool after machining the BMG [42]

The aforementioned state-of-the-art studies have been conducted with various kinds of BMGs, including Zr-based and Cu-based. Although it still faces some difficulties and troubles in micro machining, the preliminary experiment results indicated that diamond turning is an important and flexible micro machining method for fabricating BMGs into precise and useful components [30, 42, 43, 59, 60].

3 Laser processing of BMGs

3.1 Introduction to laser micro processing

The use of laser in materials processing, machining, and medical applications is a rapidly growing area of research [44]. It is a non-traditional subtractive manufacturing process, in which a laser beam directly toward the surface of the workpiece. The energy of the laser beam is focused onto the surface of the workpiece and the thermal energy of the laser is transferred to the surface, heating, melting, and vaporizing the material. This process employs thermal energy to remove materials from metallic or nonmetallic surfaces, which is also suitable for micro machining of BMGs with low thermal conductivity [27].

Figure 13 presents the hardware configuration and working principle of the laser machining process. The machining system mainly consists of two parts, a 3D positioning linear stage and a laser source. The laser beam is emitted from the laser source and followed the controller to trace patterns onto the surface by moving x and y-direction slides. The point of the laser beam interacted with the

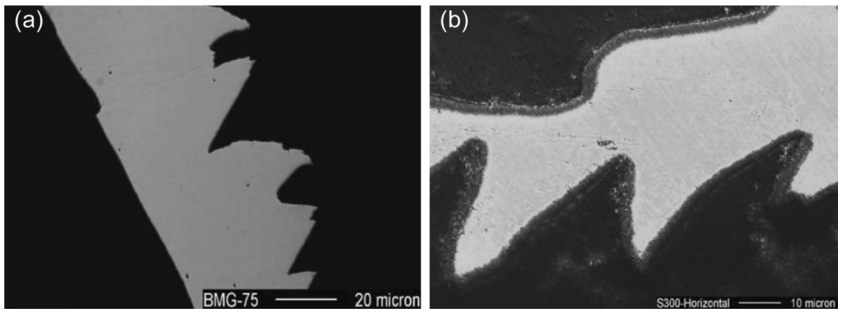

Fig. 8 Optical micrographs of polished cross-section of BMG chips machined at **a** 0.38 $m{\cdot}s^{-1}$ and **b** 1.52 $m{\cdot}s^{-1}$ cutting speed (with oxide layer) [68]

surface should be on the focal plane of the laser optical system. This focal point is very small, usually perhaps less than a fraction of a millimeter. Only the area inside the focal point is significantly affected when the laser beam passes over the surface. The interaction between the laser and the surface is illustrated in Fig. 13b.

Besides their attractive mechanical properties, the amorphous structure of BMGs leads to favorable conditions for their processing using laser micro machining. In particular, recent advances in ultrashort pulsed laser ablation as a fabrication technology of interest for generating microscale features on BMG surfaces have attracted great attention [69], which allows the specific energy deposition on a micrometer scale region with high processing speed. Unlike conventional continuous laser process, the pulsed laser irradiation can largely avoid severe crystallization and oxidation in machining process by large reduction of thermal effect area [70]. Therefore, taking features of low cost, flexible installation, and easy maintenance especially for the nanosecond pulsed laser system, laser processing has become a versatile tool and interesting focus for micro machining of BMGs.

3.2 Surface microstructures after laser point shot

Materials respond differently to various kinds of energy, and the structures left on the irradiated surface will uncover the thermal phenomena that take place when processing BMGs with pulsed laser irradiation. The lack of grain boundary and low thermal conductivity gift the BMGs superiority over some conventional crystalline alloys by laser machining [71]. As BMGs are very sensitive to temperature variation and shielding gas, the thermal process during laser machining may result in crystallization and oxidization of BMGs, further affecting the properties of BMGs [50]. It is, therefore, necessary to determine which parametric combination results in retaining the initial amorphous structure as well as producing a clear pattern with an acceptable removal rate.

In 2010, Ma et al. [72] investigated the response of a Zr-based BMG ($Zr_{55}Al_{10}Ni_5Cu_{30}$) to a Ti-sapphire femtosecond pulsed laser. Three different types of surface microstructures with permanent concentric rings were produced through varying laser fluences and shot numbers. As a single-shot ($N = 1$) femtosecond laser was fired at the target, two distinct surface topographies were generally observed at different laser

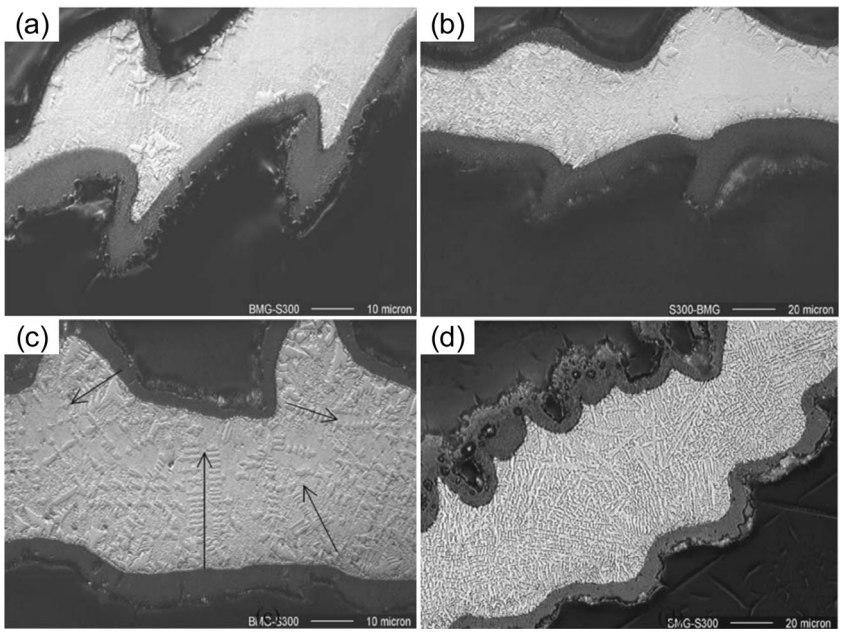

Fig. 9 Optical micrographs of the polished and etched BMG chips obtained at 1.52 $m{\cdot}s^{-1}$ cutting speed: **a** crystallization incipient next to oxide layer; **b** transition from crystalline (left) to amorphous (right) regions; **c** dendritic crystalline branch and the maximum cooling rate directions indicated by arrows; and **d** fully crystalline region [68]

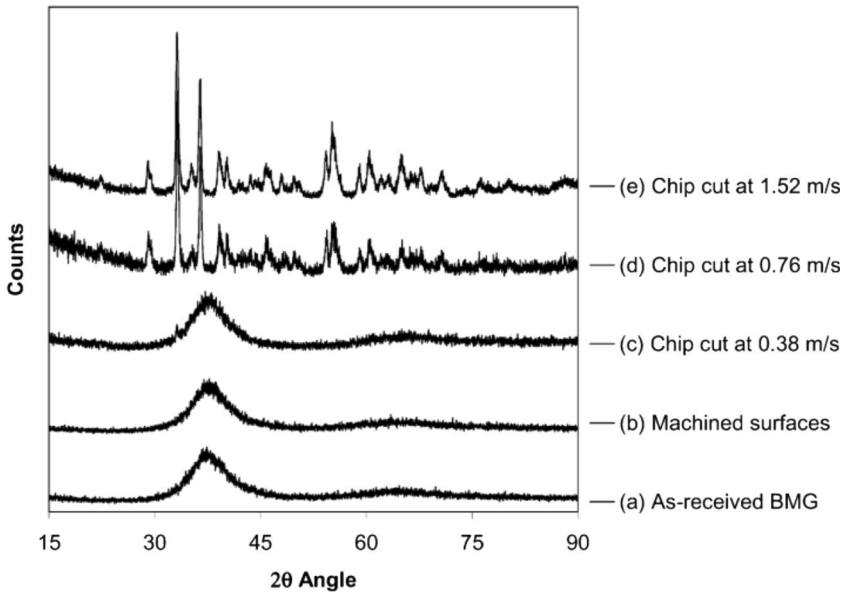

Fig. 10 X-ray diffraction analysis results for as-received, machined surface, and chips of BMG obtained with different speeds [68]

fluences, as shown in Fig. 14. In the case of low laser fluence, some random structures were generated on the laser spot including nanocavities and nanorims, but with little melting traces. While at the high laser fluence, some re-solidified liquid flow resulted in bulges at the irradiation center, which could be originated from the strong thermal ablation processes [73].

When the BMG sample was irradiated by femtosecond laser with multiple pulses accumulation, the evolvement processes of periodic surface microstructures was variable with different laser parameters. As shown in Fig. 15a, when the accumulated laser shots were $N = 30$ with the laser fluence of $F = 0.18$ J·cm^{-2}, ripple structure appeared on the laser spot. Alike to the previous observations reported by many other groups, the laser-induced ripples were orientated perpendicular to the direction of the incident electric field [74–76]. Furthermore, at the center of the spot, a circular hole with diameter of about 2 μm was formed, which may attribute to the reduced damage threshold of the surface with gradual accumulating of laser shots, or the incubation effect of multiple-pulse striking became predominated. In the case of high laser fluence of $F = 2.82$ J·cm^{-2}, the formation of subwavelength ripples with thermal melting background appeared in the periphery of the ablated zone, as shown in Fig. 15b. Further analysis of the subwavelength ripples showed some differences. The ring interval increased at the laser fluence of 2.82 J·cm^{-2}, while it decreased at the laser fluence of 0.18 J·cm^{-2}. This sharp contrast suggested that the formation of the two types of concentric rings was due to different physical mechanisms. The morphological evolution of the surface under the irradiation of multi-pulse femtosecond lasers with the mediated energy fluence of 1.2 J·cm^{-2} showed that the radial change of this mixed concentric pattern was located between the high and low laser fluence patterns, as shown in Fig. 15c.

Surface rippling patterns were further observed on the irradiated surface of BMGs by using the nanosecond pulsed laser. For example, Liu et al. [77] reported the ripple patterns in the nanosecond pulsed laser irradiated area of Vit 1 BMG with single shot, as shown in Fig. 16. They attributed this surface rippling phenomenon to the Kelvin-Helmholtz (K-H) instability at the interface between the molten layer and the expanding plasma plume, which was very similar to the unstable interface between the wind and the water when

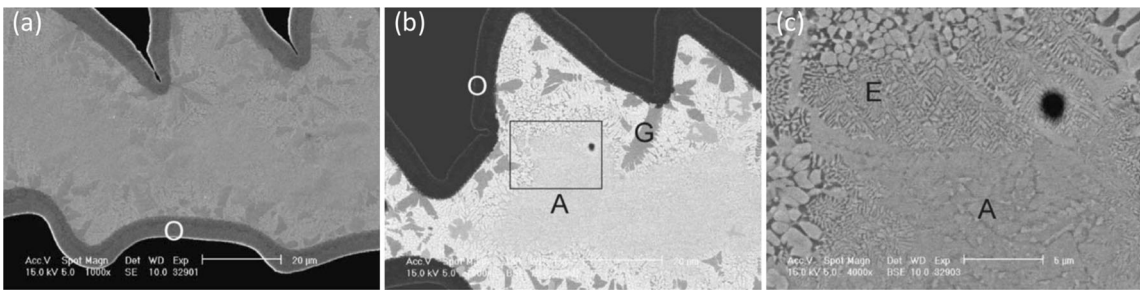

Fig. 11 FESEM micrographs of the chip cross-section: **a** contrast adjusted to show the oxide layer surrounding the chips, (O); **b** contrast adjusted to show the inside crystalline and amorphous regions, (G) represents the gray leaf-shape crystalline region; and **c** close-up view of the box in **b** with the amorphous (A) to eutectic (E) crystalline transition [68]

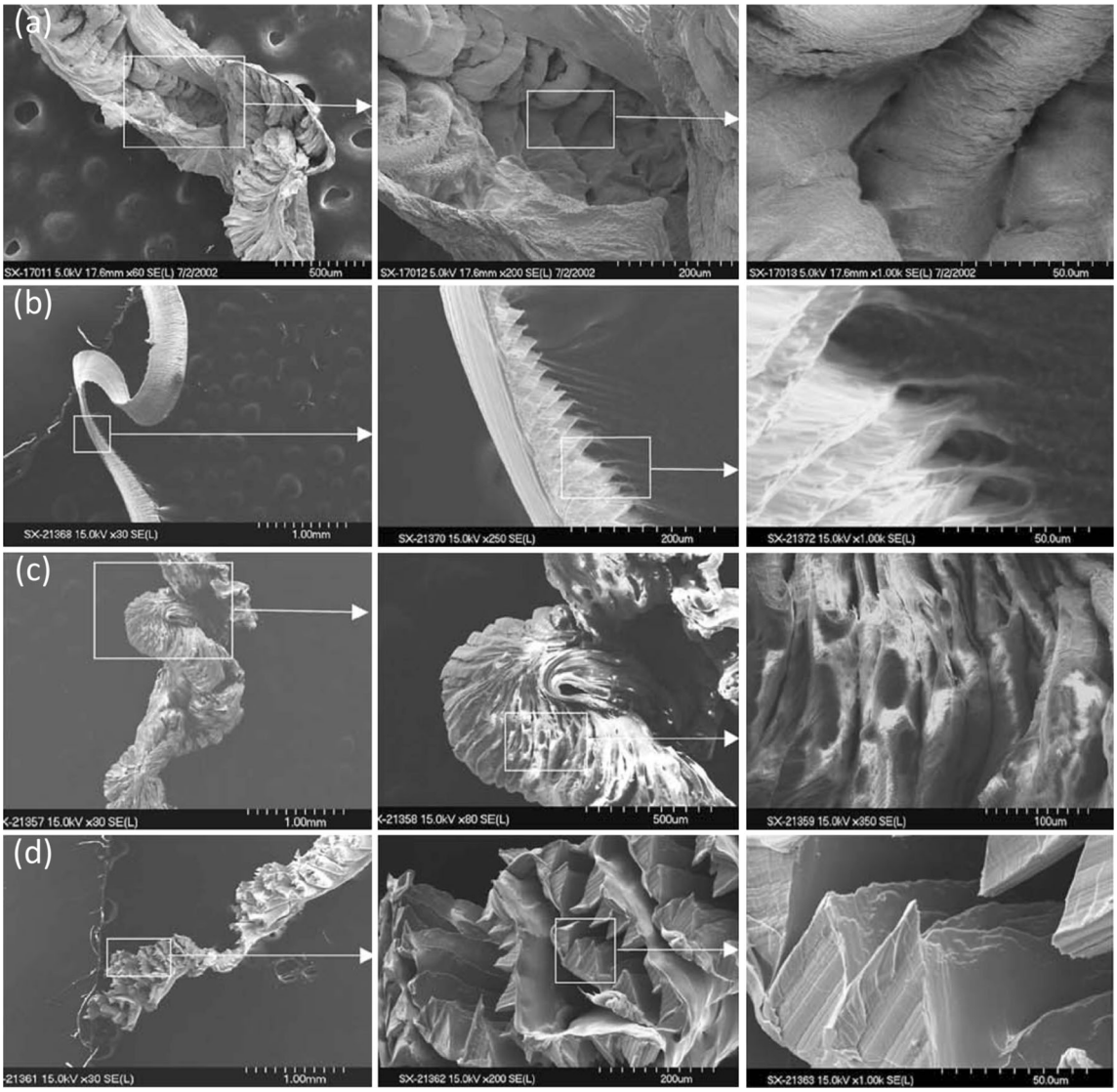

Fig. 12 SEM micrographs of BMG chips machined at 1.52 $m \cdot s^{-1}$ cutting speed: **a** Tool: WC-CVD, with chip light emission; **b** Tool: WC-PVD, no chip light emission; **c** Tool: PCBN, with chip light emission; and **d** Tool: PCD, no chip light emission [42]

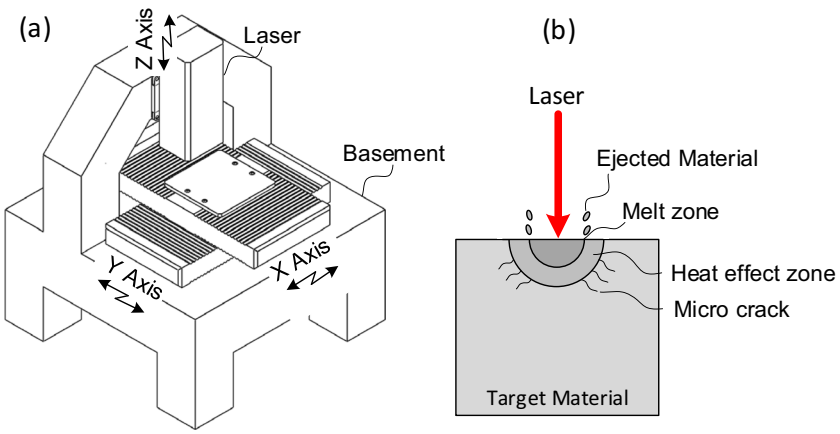

Fig. 13 Schematic diagrams of **a** laser processing on three-axis precision stage, and **b** laser-material interaction

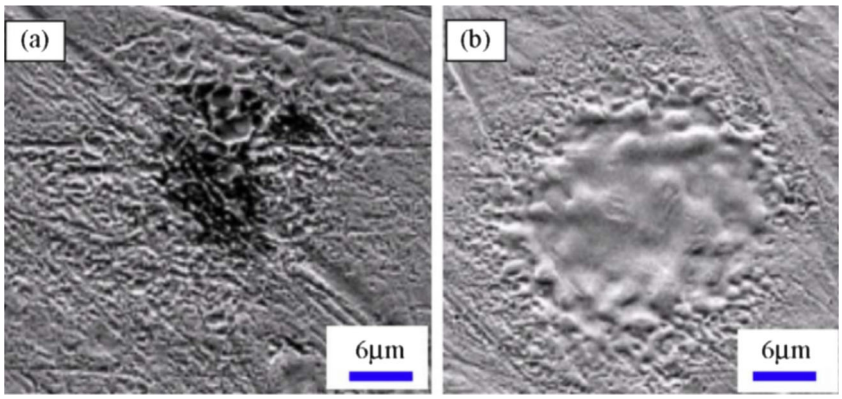

Fig. 14 Surface topographies on the metallic glass irradiated by a single-shot femtosecond laser ($N = 1$) with two different energy fluences: **a** $F = 0.18$ J·cm^{-2} and **b** $F = 3.53$ J·cm^{-2} [72]

the wind skittered over the water surface. Thus, the molten Vit 1 worked as the "water," and the expansion of the high-pressure plasma generated the "wind." For pulsed laser irradiation of Vit 1 with high intensity, the velocity of Vit 1 melt could be regarded as zero compared to that of plasma plume [78]. The density of Vit 1 in the liquid state was much greater than that of plume [79, 80], and the viscosity of Vit 1 melt was much larger than of plume [81]. Taken these into consideration, the ripple spacing was actually determined by the density and initial horizontal velocity of the expanding plasma for fixed surface tension, as shown in Fig. 17.

Furthermore, similar experiments, with the same BMG and laser source, were conducted within water environment [82]. The surface rippling was also observed around the crater edge with a star-shaped pattern, namely Saffman-Taylor fingering, as shown in Fig. 18. This was explained by perturbation analysis, the instability between the plasma plume and the molten BMG.

When Vit 1 BMG was irradiated by using a high-power nanosecond laser pulse, a unique porous structure as shown in Fig. 19 was further reported [83]. Ripples being similar to those in Fig. 16 were also observed at the edge of the irradiated area as shown in Fig. 19a. Moreover, porous structures with 100-nm scale voids were homogeneously distributed at the entire irradiated region as shown in Fig. 19b–f, and their formation was theoretically ascribed to a liquid-gas spinodal phenomenon.

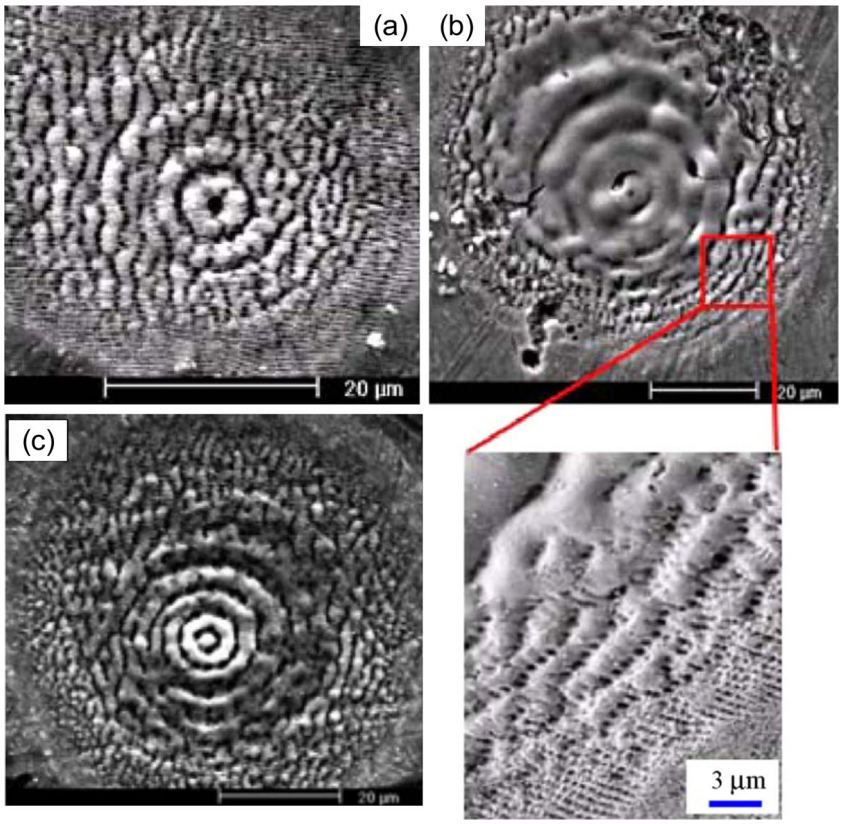

Fig. 15 Surface morphologies of the BMG irradiated by multiple-pulsed $N = 30$ femtosecond lasers at **a** low energy fluence of 0.18 J·cm^{-2}; **b** high energy fluence of 2.82 J·cm^{-2}; and **c** mediated energy fluence of 1.2 J·cm^{-2} [72]

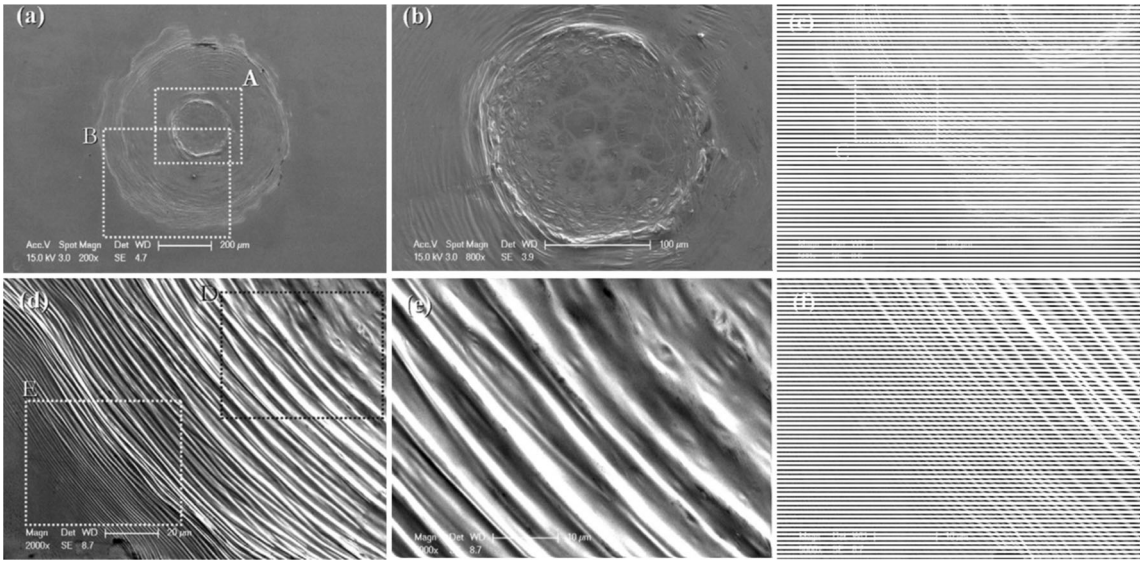

Fig. 16 The irradiated morphologies of Vit 1 BMG by a nanosecond pulsed laser with singe shot: **a** the full view of irradiated area; **b** concentrated ablated region marked by "A" in **a**; **c** a close-up view of the area "B" in **a**; **d** an enlarged view of the area "C" in **c**; **e**, **f** correspond to the areas "D" and "E" in **d**, respectively [77]

Williams et al. [69] further investigated the interaction between a nanosecond pulsed laser with the Vit 1 BMG. Different pulse lengths, ranging from 15 to 140 ns, were examined when delivering single pulse to BMG surface using a Yb fiber laser system. The authors introduced a thermal model to predict the temperature evolution during laser processing. For example, Fig. 20 illustrated the temperature evolution with the time for different pulse length at a fixed fluence of 14 J·cm^{-2}, calculated by the theoretical model. For short pulse length, high peak laser power resulted in wide melt pool and more melt ejection surrounding the crater, as shown in Fig. 20. Furthermore, surface ripples were also observed immediately outside the edge of the crater as shown in Fig. 21, where the temperature was subjected to heating above the glass transition temperature of the material (T_g) but below the melt temperature.

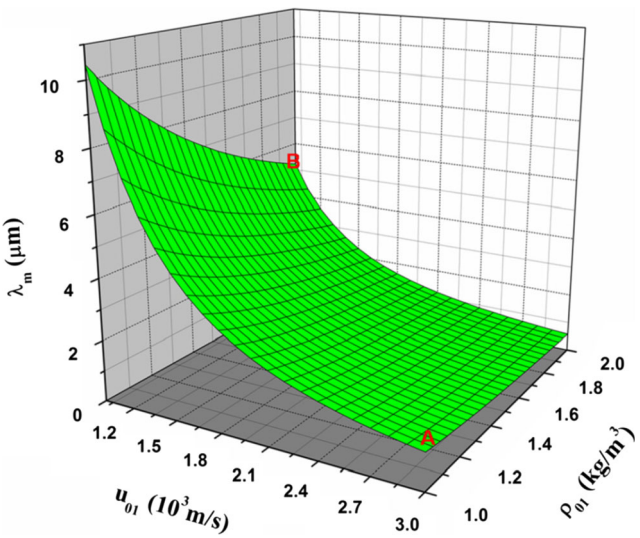

Fig. 17 Prediction of ripple spacing λ_m with the change of density ρ_{01} and initial horizontal velocity u_{01} of the expanding plasma [77]

3.3 Surface microstructures after laser line processing

By laser point shot as mentioned in Section 3.2, various microstructures such as ripple, Saffman-Taylor fingering, and porous nanostructure are generated on BMG surfaces in laser processing. For practical applications, large-area surface microstructures are necessary and thus large-area laser irradiation, pulse by pulse and line by line, is required. Some progresses are also achieved recently in laser line processing of Vit 1 BMG.

By laser line irradiation in vacuum, Huang et al. [84] reported that hierarchical micro/nano structures were generated on the surface of Vit 1 BMG, which consisted of two layers, a layer of micron-scale laser pulse tracks covered by a cotton-like MG thin film with nanometer-scale micro structure, as shown in Fig. 22. The formed surface microstructures significantly increased the effective surface area which had the potential to enhance the applications of BMGs in heterogeneous catalysis and biomedical engineering. Furthermore, the effects of laser irradiation parameters such as laser power and scanning speed on the surface microstructures were also explored. Experimental results showed that hierarchical micro/nano structures could be generally generated at the irradiated area but the detailed surface microstructures were dependent on the laser parameters in some degree. By XRD analysis, it was confirmed that the laser line irradiated surface retained an amorphous feature. By theoretical and experimental analysis, the formation mechanism of the hierarchical micro/nano

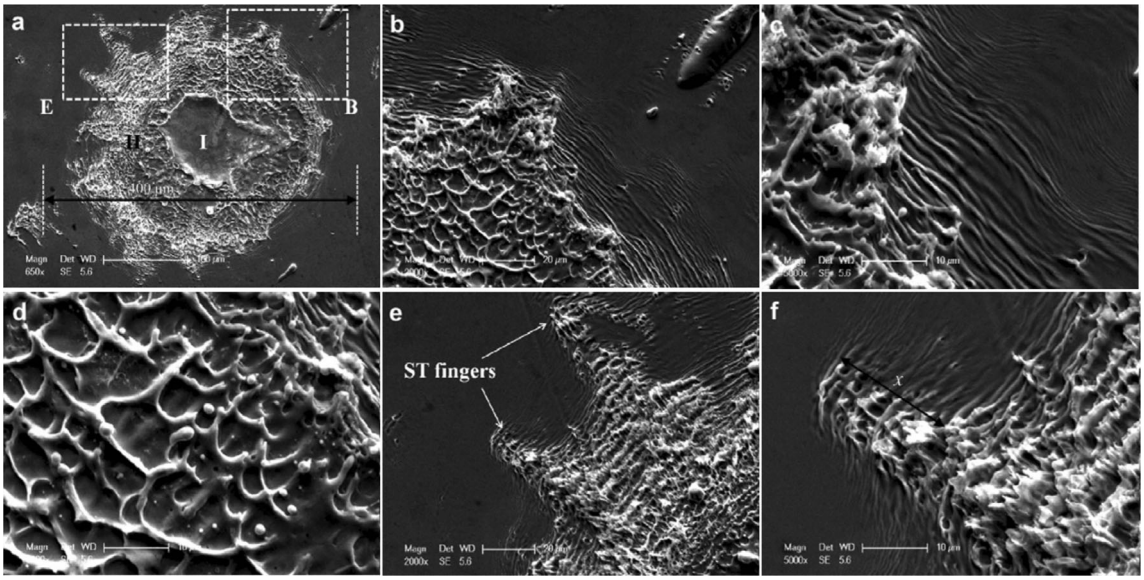

Fig. 18 Surface morphologies of Vit 1 BMG irradiated by a nanosecond pulse laser with singe shot in a water environment: **a** the full view of irradiated area consisting of a smooth region "I" and a rough region "II"; **b**–**d** close-up views of the area "B" marked in **a** at different magnification; **e**, **f** correspond to the area "E" in **a**, showing the Saffman-Taylor fingering [82]

structures was further discussed which was related to heating, liquefaction, vaporization, cooling, and re-deposition processes during the laser line irradiation.

Shield gases such as argon and nitrogen have been widely employed previously during laser processing of BMGs to avoid surface oxidation and crystallization, but their effects on the laser-BMG interaction were revealed recently. By comparative experiments in argon and nitrogen shield gases using single line irradiation, Huang et al. [85] reported that compared to argon gas, the formation of cracks in the irradiated area of Vit 1 BMG was greatly enhanced when using nitrogen gas as shown in Fig. 23. By XRD and Raman analysis as shown in Fig. 24, the enhanced crack formation in nitrogen was ascribed to the formation of ZrN that enhanced the thermal mismatch between the molten layer and the substrate, further resulting in high thermal stress at their interface during re-solidification.

Although cracks are commonly bad thing for material surface, they were used to generate hierarchical micro/nano structures on the surface of Vit 1 BMG by using multi-line laser irradiation [86], as shown in Fig. 25. Three kinds of surface structures, micro grooves, cross-shaped protrusions and nanoparticles, were observed, which were dependent on the laser parameters such as the laser power, scanning speed, and pulse overlap rate. Especially, the cross-shaped protrusions were firstly reported, and their formation was ascribed to the selective thermoplastic extrusion of the BMG material out of the cracks and laser pulse tracks because of their higher absorption of laser energy and localized thermal resistivity than those of surrounded bulk material.

Laser processing exhibits the potential ability to solve some critical problems in the applications of BMGs [27]. For example, it can be used to fabricate complex geometries free of using expensive molds, satisfying more complex or customer-designed applications. More studies on this interesting topic will further improve the flexibility on micro machining of BMGs.

4 Micro electric discharge machining of BMGs

4.1 Introduction to micro-EDM

Among a variety of micro machining methods, micro-EDM provides some unique advantages, such as the capability of fabricating high aspect ratio and complex 3D shapes [52]. It is therefore potentially suitable for manufacturing some complex surfaces with large aspect ratio, such as micro-holes and micro-pillars in miniature devices with flexibility.

Micro-EDM is a novel kind of manufacturing process that derives from conventional die EDM sinking and wire EDM cutting processes, in which the desired shapes can be fabricated by using electrical discharges [87]. The micro-EDM tool is one of the electrodes rotating at high speed in the dielectric oil and removing the work piece material by sparking. The tool electrode is precisely positioned by three-dimensional linear stages. The hardware configuration is shown in Fig. 26. The sparks occur at the tip of the tool electrode to remove the material without cutting forces. Since it is also a typical non-contact machining method, micro-EDM is considered suitable for micro machining and to be one of the feasible ways to produce micro/nano structures on hard-brittle materials.

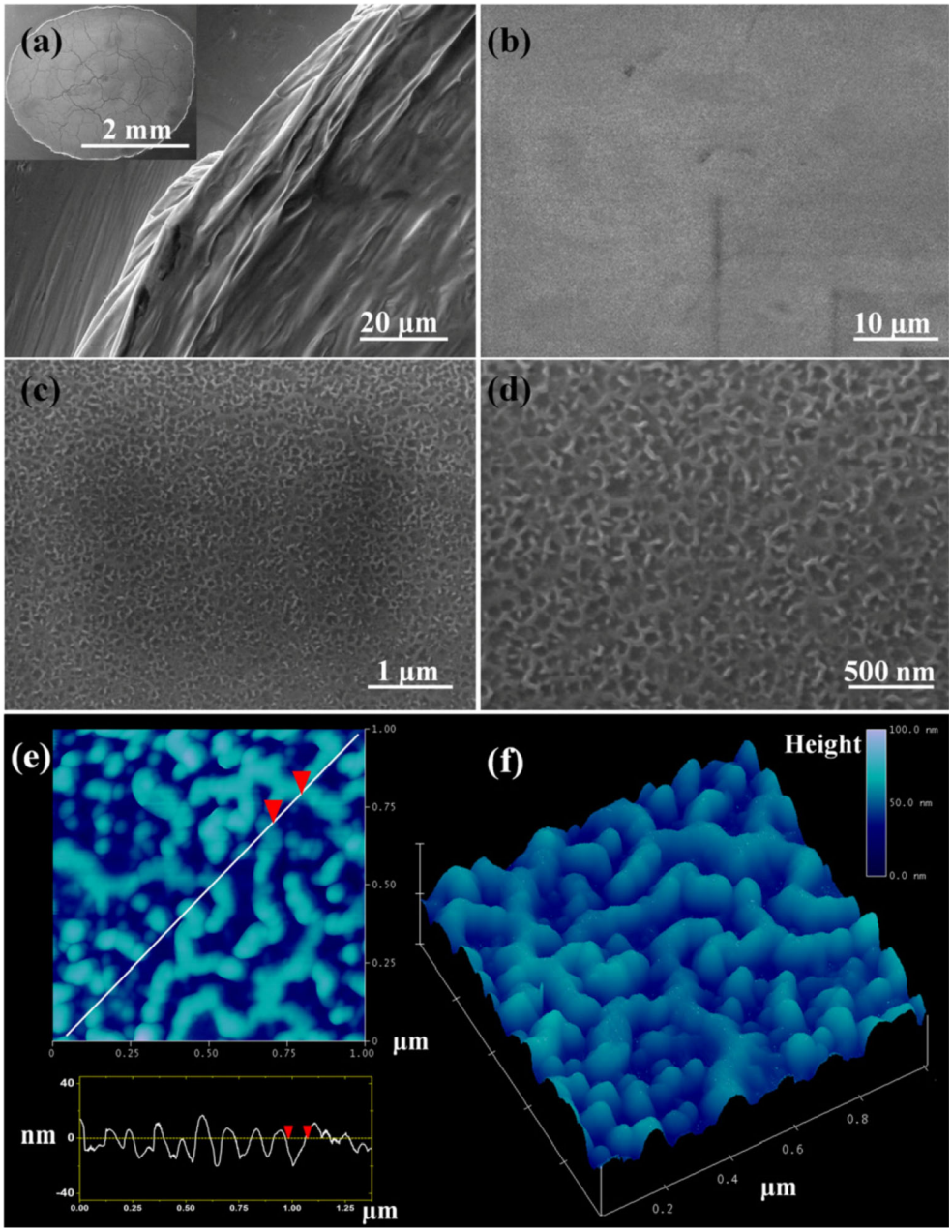

Fig. 19 Surface morphologies of Vit 1 BMG in the irradiated area after single shot by using a Nd:YAG nanosecond pulsed laser with high laser power [83]

The micro-EDM method has the capability of machining electrical conductive materials, including most of the metals, without considering the hardness, strength, and temperature-resistant [88]. Moreover, it is widely used to produce micro-scale components and structures, such as micro-molds, micro-dies, microprobes, micro-tools, thin sheet materials, and some complex 3D shapes with high accuracy and fine surface roughness. Thus, micro-EDM is also a potential method to shape BMGs for specific applications such as microfluidic channels. Up to now, some fundamental studies have been conducted to advance the understanding of the material removal process of BMGs during micro-EDM.

4.2 Surface microstructures after micro-EDM

Recently, there have been a few investigations on the machining performance of BMGs by micro-EDM. Micro-EDM is intrinsically an electro-thermal process, involving material heating, melting, vaporization, and re-solidification. Similar to laser processing, any unsuitable parameters could result in unpredictable heating and cooling process, leading to crystallization and oxidization of BMGs. Therefore, some studies were focused on the effects of the discharge voltage and capacitance on the material removal rate, cross-sectional profile, surface morphology, and finish roughness [89].

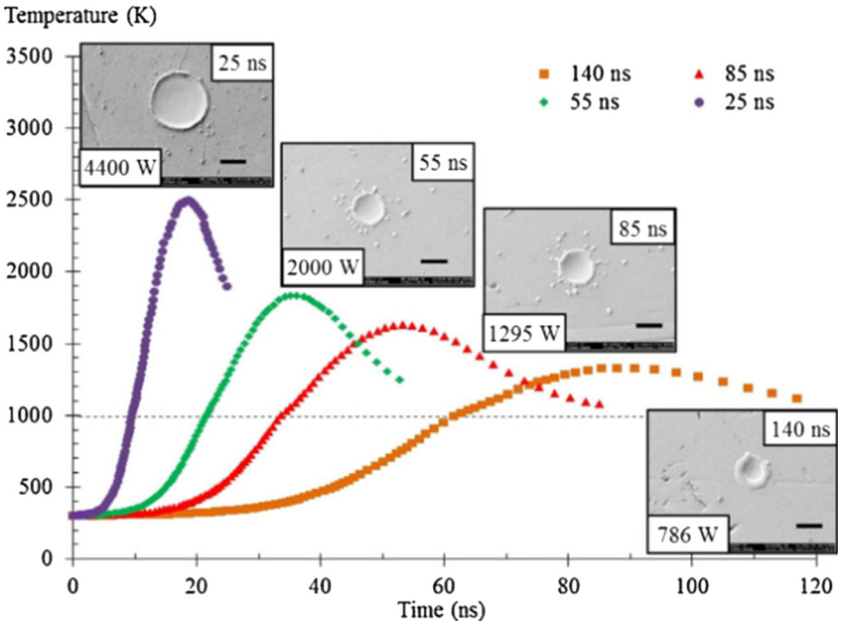

Fig. 20 Evolution of temperature predicted by the theoretical model at a fluence of 14 J·cm^{-2} [69]

Yeo et al. [90] conducted a series of experiments to demonstrate the feasibility of using micro-EDM for fabricating microgrooves and microslots on Zr-based BMG surface. Two input energies and three kinds of tool electrodes were employed in the experiments to investigate the effects of various machining parameters on the surface quality. The micrographs of the machined surface, as shown in Fig. 27, indicated that using a lower input energy significantly reduced the burr width and surface roughness. Moreover, at low input energy setting, it showed that tube-shaped electrodes presented lower tool wear ratio than rod-shaped electrodes because of large tool electrode area exposed to the dielectric that enhances the heat transport.

Chen et al. [91] evaluated the machining performances of micro-holes and 3D microstructures on three kinds of BMGs during micro-EDM, including $La_{62}Al_{14}Ni_{12}Cu_{12}$, $Zr_{55}Al_{10}Ni_5Cu_{30}$, and $Cu_{46}Zr_{44}Al_7Y_3$, by using X-ray diffraction, scanning electron microscopy, and nanoindentation. Figure 28a–c illustrated the top views of micro-holes drilled by micro-EDM on these three BMGs, and panels d–f of Fig. 28 were the amplified edge morphologies images of Fig. 28a–c, respectively. On the edge of micro-hole on $La_{62}Al_{14}Ni_{12}Cu_{12}$ substrate, three different zones can be seen, the recast layer (zone 1), the heat-affected zone (zone 2), and the base material zone (zone 3), as shown in Fig. 28d. The recast layer (zone 1) showed some extensive surface debris and a lot of actinomorphic stripes concentrated in the heat-affected zone (zone 2). The $Zr_{55}Al_{10}Ni_5Cu_{30}$ substrate showed less burrs surrounding the edge of the micro-hole and the heat-affected zone appeared dark as shown in Fig. 28b. The edge of the micro-hole on the $Cu_{46}Zr_{44}Al_7Y_3$ substrate was much better than the other two BMGs stated above. Little recast debris and heat-affected zone can be found on the edge of micro-hole. Furthermore, by measuring the indentation hardness around the holes, the authors concluded that no crystallization occurred for these BMGs during micro-EDM, but more direct evidence was not provided.

Based on the previous studies, Huang et al. [92] systematically investigated the micro-EDM machining performance of Vit 1 BMG. Results of orthogonal experiments indicated that experimental parameters such as discharge voltages and capacitances strongly affected the material removal rate, cross-sectional profile, surface morphology, and roughness. In general, reducing the discharge voltage and capacitance resulted

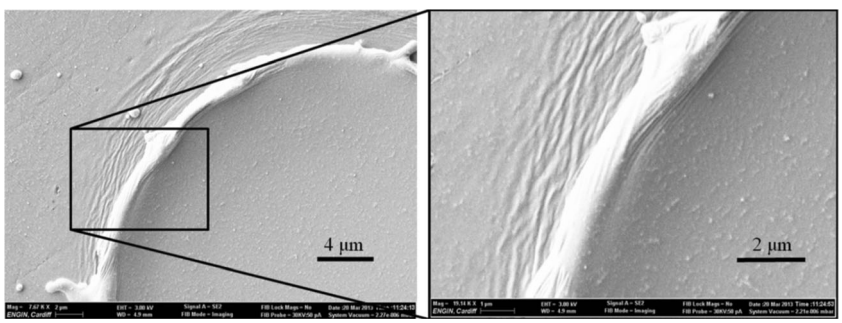

Fig. 21 SEM micrographs of a crater obtained with a pulse length of 15 ns and fluence of 7.6 J·cm^{-2} [69]

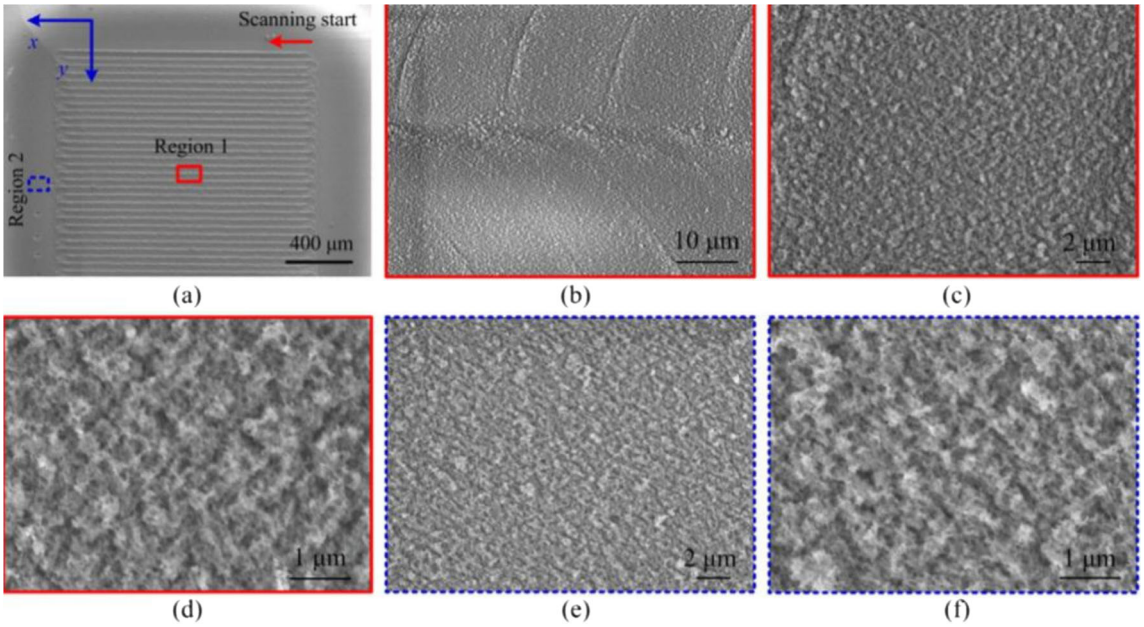

Fig. 22 SEM morphologies of Vit 1 BMG in the irradiated area at different regions and magnifications [84]

in low surface roughness, but the material removal rate was also decreased. By analyzing the SEM morphologies after micro-EDM, it was seen that the machined surface was distributed with many randomly overlapped craters with various size. The size of the crater was significantly dependent on the discharge voltage and capacitance as shown in Figs. 29 and 30, which were obtained at various capacitances and voltages. Using a circle to surround the crater, the size of the crater was evaluated quantitatively. It showed that for the same voltage of 90 V, the diameter of the crater was decreased from 13 to 5 μm with decreasing of capacitance from 3300 to 220 pF; for the same capacitance of 3300 pF, the diameter of the crater was also decreased from 17 to 11 μm with decreasing of voltage from 110 to 70 V. Accordingly, smaller craters could be formed at low discharge voltage and capacitance, resulting in better surface quality, but the machining efficiency will also be low. So, for practical applications, the parameters for micro-EDM should be optimized.

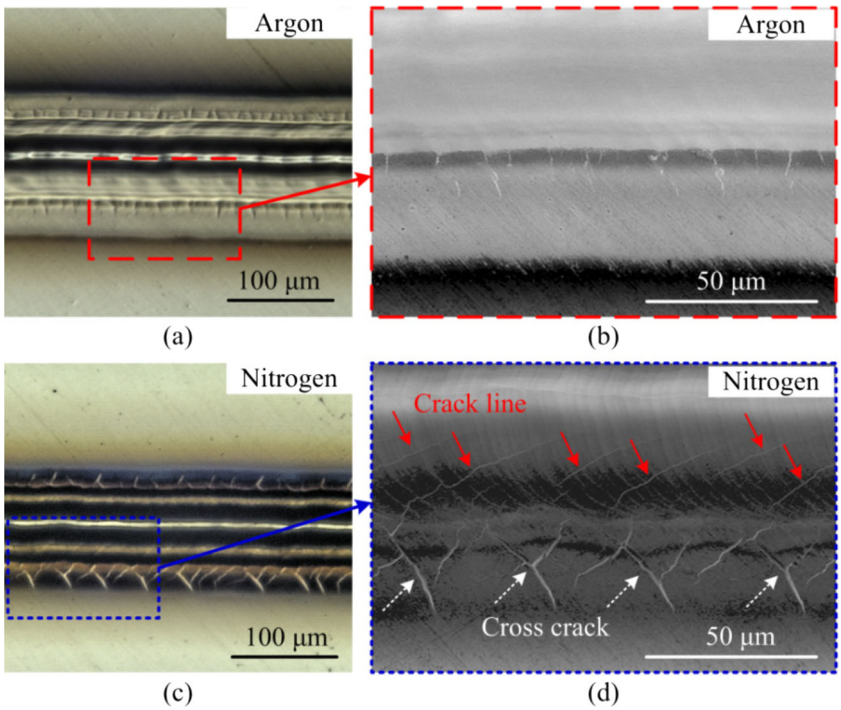

Fig. 23 Optical morphologies of Vit 1 BMG after single line laser irradiation using different shield gases: **a**, **b** argon; **c**, **d** nitrogen [85]

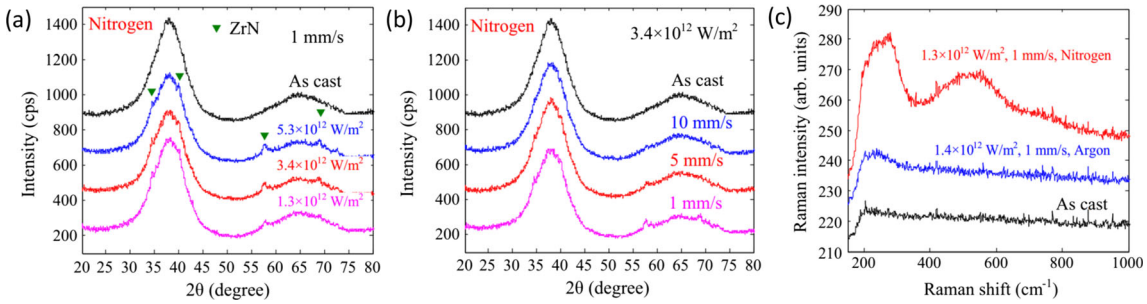

Fig. 24 **a**, **b** XRD patterns and **c** micro-Raman spectra obtained in the irradiated areas of Vit 1 BMG [85]

4.3 Crystallization and carbonization

In 2013, a study by Hsieh et al. [55] indicated that significant crystallization had occurred when machining a $Zr_{38.5}Ti_{16.5}Cu_{15.25}Ni_{9.75}Be_{20}$ BMG by the conventional EDM in kerosene. Some ZrC and TiC phases were observed in the recast layer of the EDMed surface, hardening the surface. Compared to the conventional EDM, although the discharge energy for micro-EDM is very low, it is still an electro-thermal material removal process. Thus, crystallization issue should be also carefully considered for micro-EDM of BMGs because they are quite sensitive to temperature variation in process.

In this aspect, Huang et al. [92] investigated the surface crystallization and carbonization of Vit 1 BMG after micro-EDM in EDM oil (CASTY-LUBE EDS). Raman spectra and XRD patterns demonstrated that amorphous carbon and ZrC phase existed on the micro-EDMed surface although the ZrC crystalline peaks were very weak as shown in Fig. 31. It should be noted that compared to the conventional EDM, the micro-EDMed surface retained better amorphous feature because of the very low discharge energy, exhibiting the potential for micro machining of BMGs.

Furthermore, the formation of ZrC phase in micro-EDM was further analyzed [92]. As illustrated in Fig. 32, during the pulse-on, the sparks occurred between the copper electrode and Vit 1(Zr-based) BMG made the molten or vaporized BMG suspended in the EMD oil, which further connected to the hydrogen and carbon decomposed from the oil. During the pulse-off, some ZrC was formed during the cooling and re-solidifying processes because of the high chemical affinity between Zr and C atoms.

Up to now, as a young group of metallic alloys, the research on micro-EDM of BMGs has attracted a lot of

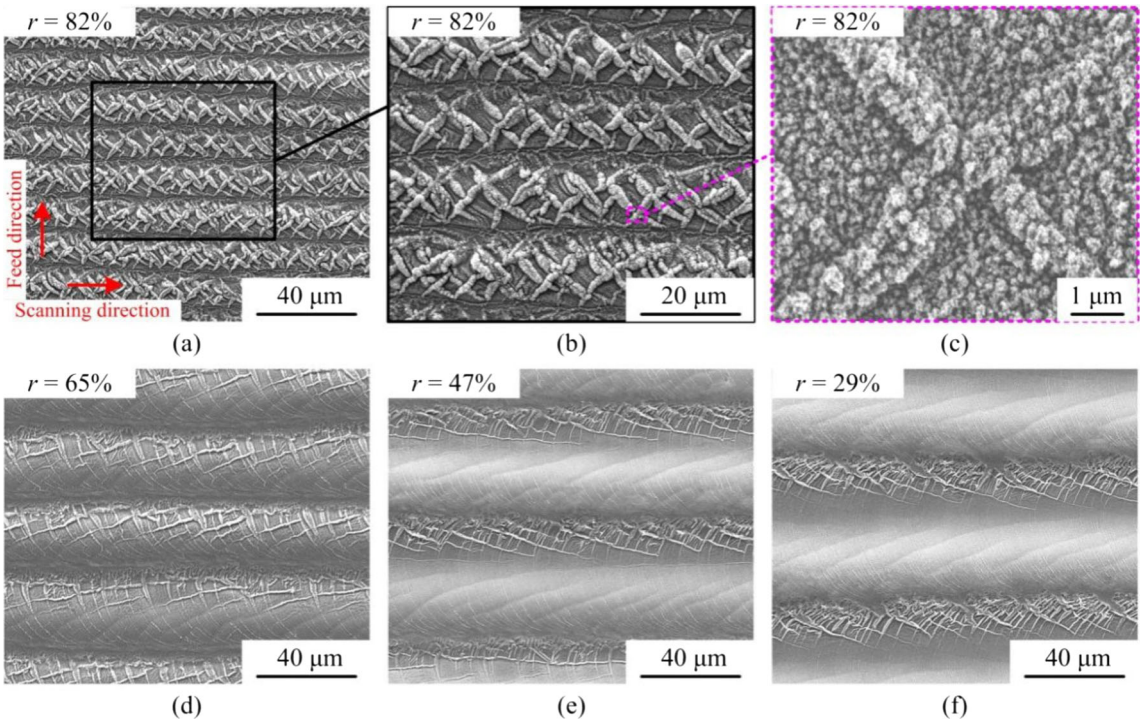

Fig. 25 SEM morphologies of Vit 1 BMG in the irradiated area under various pulse overlap rates *r* [86]

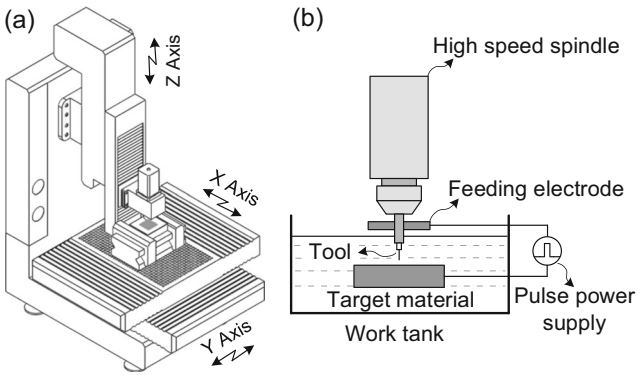

Fig. 26 Schematic diagrams of **a** hardware configuration of micro-EDM machine and **b** working principle of micro-EDM

attention. As stated above, some new phenomena in the machining were observed and great success was achieved in this field. However, the research on this topic has not been widely conducted, and the fundamental mechanism during micro-EDM of BMGs has not been understood completely. In addition, like the conventional EDM, crystalline phases appeared on the machined surface. Thus, subsequent machining process for example grinding may be required to remove the crystalline layers for obtaining a totally amorphous surface [93].

5 Potential applications of micro-/nano-fabricated patterns

Due to the outstanding thermal formability of BMGs in the supercooled liquid region, thermoplastic forming technology has recently been exploited for forming BMG components with micro/nano-structured surfaces [1, 24, 29]. The unique superplasticity within the supercooled liquid region opens an alternative window for micro machining of BMGs, but it also possesses some inherent disadvantages. For example, it is difficult to control the shaping temperature and rate in TPF because of the narrow supercooled liquid region. Any deviation would possibly lead to crystallization and oxidation. On the other hand, the TPF technology generally has high cost and requires robust and durable masks or molds. Additionally, it is also lack of the capability on real 3D surface texture manufacturing. Thus, alternative techniques which could operate at extensive temperature and also generate complicated surfaces with fine accuracy and high surface quality are desired.

As reviewed in the foregoing sections, these three methods, based on material removal principle, are promising methods that replenish the deficiency of TPF process on versatile structure fabrication for BMGs. The diamond turning, as a very promising technique for ultra-precision machining, is gifted with the inherent advantages on freeform generation with high profile accuracy together with fine surface integrity, especially for some optical reflective/refractive surfaces. Through diamond turning, atypical sinusoidal grid surface was generated on a Zr-based BMG to demonstrate the feasibility of diamond turning on BMGs by Zhu et al. [30]. From the measurement results, the machined harmonic microstructured surface with no defects was obtained, and the roughness of the machined surface was about 0.13 μm. The outstanding durability of BMGs and high finish surface quality motivate the wide application of diamond turning in mold fabrication, which have been identified as promising alternative materials for steel molds. Pan et al. fabricated an aspherical microlens array on an oxygen free copper substrate using ultra-precision machining [94]. By using molding process, the microstructure was replicated onto BMG as shown in Fig. 33, which was further used for hot embossing on polymethylmethacrylate (PMMA) sheets for replication process. The final replicated PMMA showed good replication on geometry profile and surface quality. Molding process by using BMG material as a secondary mold can be more cost-effective and time-saving than the traditional manufacturing process does. Thus, the diamond turning shows great potential on mold fabrication with micro-/nano-structures on BMGs for hot embossing microlens array and microchannel geometries with potential application in precise optics and microfluid.

The unique mechanical properties of BMGs and their excellent micro-/nano-geometrical transferability in the supercooled liquid state exhibited great potential in the

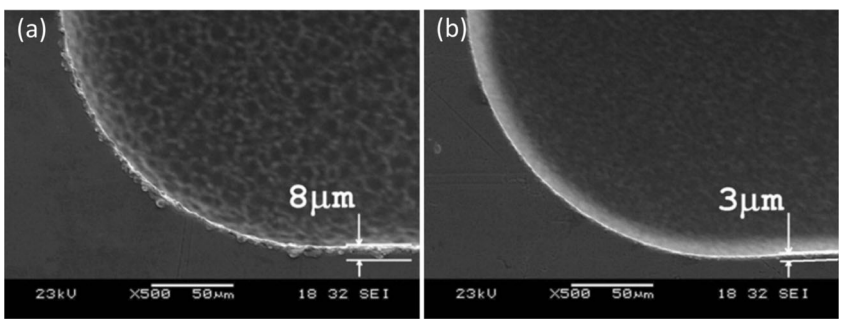

Fig. 27 Burr width and surface roughness under different input energy: **a** 13.4 μJ and **b** 0.9 μJ [90]

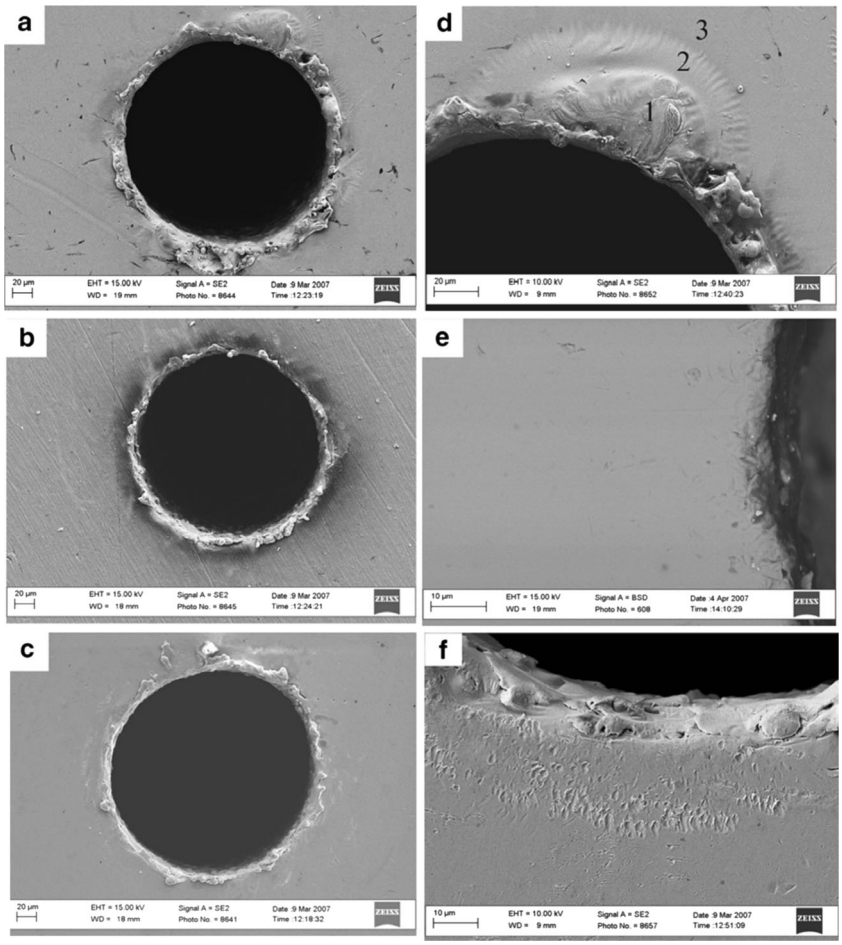

Fig. 28 SEM morphologies of the recast layer and heat-affected zone surrounding the edge of the micro-holes machined by micro-EDM on **a** $La_{62}Al_{14}Ni_{12}Cu_{12}$; **b** $Zr_{55}Al_{10}Ni_5Cu_{30}$; **c** $Cu_{46}Zr_{44}Al_7Y_3$; and **d**–**f** are the amplified edge morphologies images of **a**–**c**, respectively [91]

fabrication of super hydrophobic surfaces by laser processing. Recently, Huang et al. [86] built hierarchical micro/nano structures on Zr-based BMGs by nanosecond pulsed laser irradiation by integrating nano-, micro-, and macro-sized features in a sequential order, which endowed BMG surfaces with versatile functions for potential utilization in super hydrophobic. As shown in the comparative result in Fig. 34, the measured contact angle of the patterned BMG surface by laser processing was substantially larger than that of the as-cast BMG surface, demonstrating enhanced hydrophobicity which can extend the functional applications of BMG as structural and engineering materials.

Another interesting property of BMGs is that they have exceptional biomechanical characteristics like low elastic modulus, outstanding fracture strength, superior wear, and corrosion resistance compared to routinely used biomaterials [95]. However, the major downside of cast BMGs is their inability to osteo integrate to the surrounding living tissues. To solve this problem, Aliyu et al. [96] tried to generate a biocompatible and bone-like nanoporous layer on the BMG implant surfaces by hydroxyapatite mixed EDM. The hierarchical micro/nano structures formed on the Zr-based BMG surface were actually very similar to the micro/nano-pore of bones, which gave rise to the high biocompatibility to the surrounding tissues, as shown in Fig. 35. The machined surface was expected to facilitate higher tissue ingrowth and bone-implant adhesion. As hierarchical micro/nano structures are quite easy to be generated on BMG surface by laser processing and micro-EDM, these two micro machining methods could be widely employed to enhance the applications of BMGs as biomaterials.

6 Summary and outlook

This review presented three important and widely employed micro machining methods in BMGs by material removal, indicating the potential capabilities for a large number of industrially relevant processes. They showed the capabilities of them to be able to satisfy the demand of advanced material manufacturing. In particular, diamond turning, as a conventional machining method, aided with precision control by multi-axis servo system, makes it attractive to process BMGs due to its superiority on accuracy geometrical shaping and near optical finished surface quality. The high heating and cooling rate inherent to laser and micro-EDM present

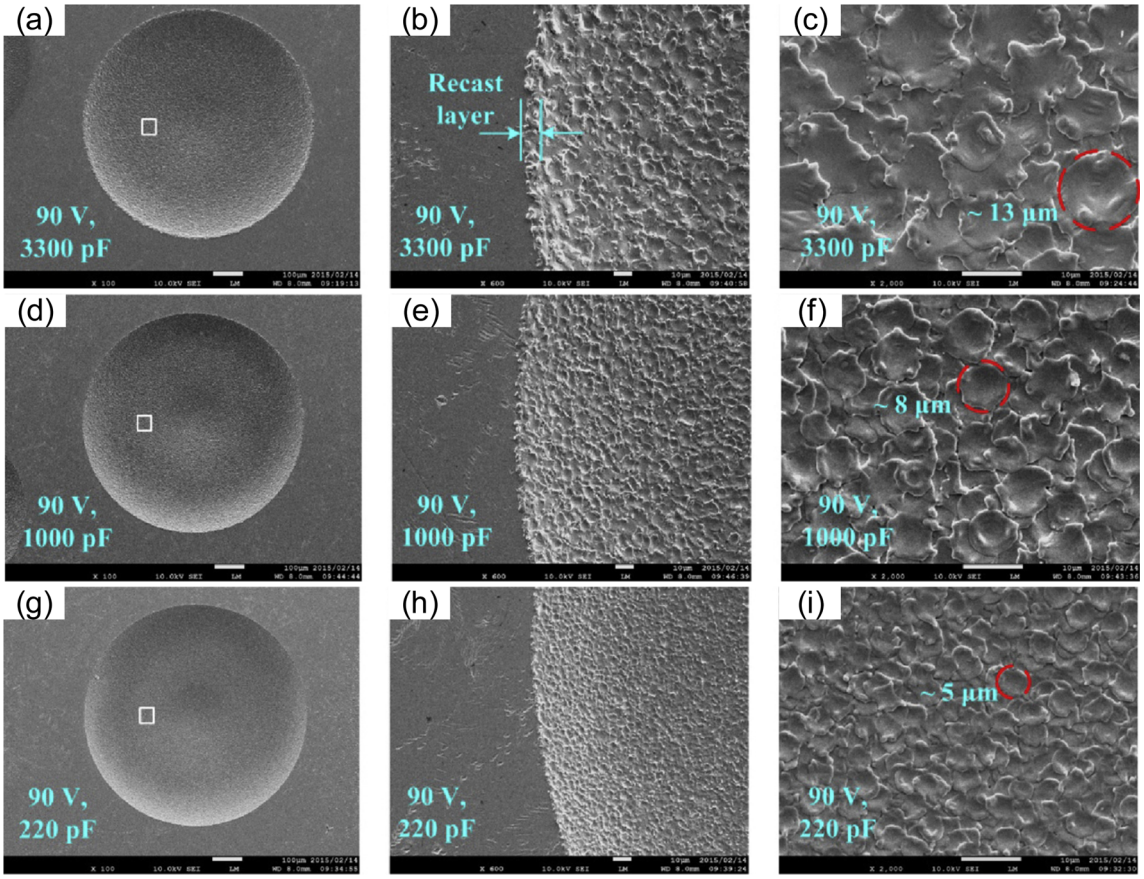

Fig. 29 Surface morphologies of the micro-EDMed holes at a voltage of 90 V and various capacitances: **a**–**c** 3300 pF; **d**–**f** 1000 pF; **g**–**i** 220 pF [92]

great potential applications on BMG micro machining because of large material removal rate and the ability to nearly retain amorphous structure. Although the research efforts on these manufacturing methods of BMG machining have increased in the past decades, our fundamental understanding of the underlying mechanism and mechanics is still far from complete. For each of the reviewed processes, we summarize as follows.

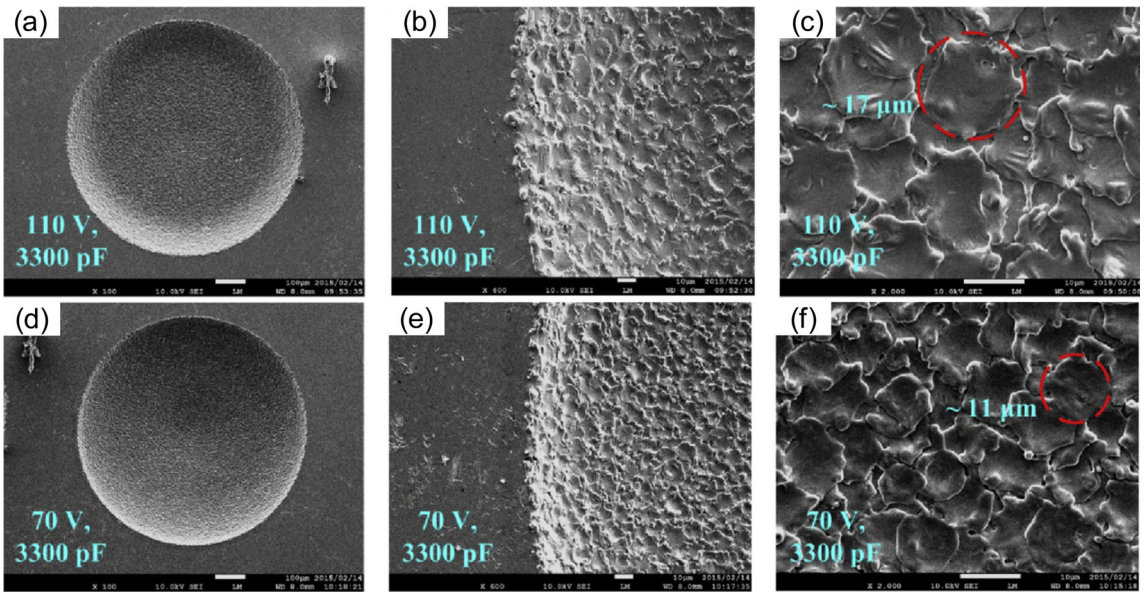

Fig. 30 Surface morphologies of the micro-EDMed holes at a capacitance of 3300 pF and various voltages: **a**–**c** 110 V; **d**–**f** 70 V [92]

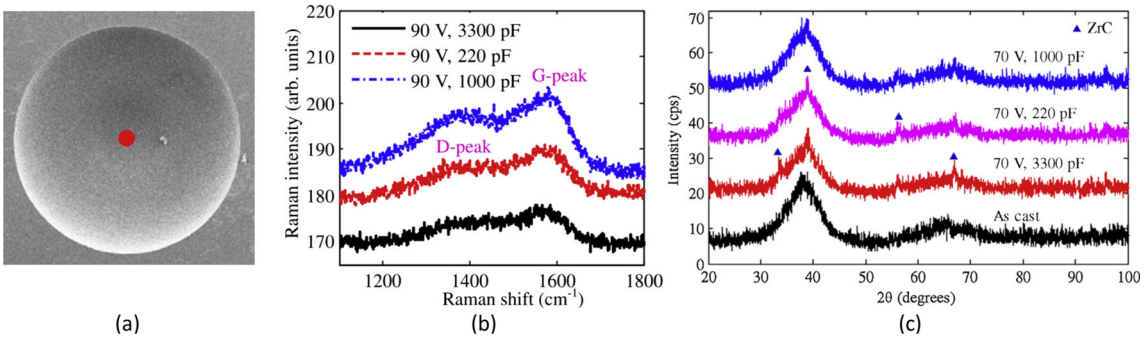

Fig. 31 Typical Raman spectra and XRD patterns of the micro-EDMed surfaces [92]

Diamond turning The lack of large-scale grain boundaries and crystal defects in BMGs makes them ideal candidates for nano-/micro-structure fabrication by convention mechanical machining methods, such as diamond turning. Investigation on the interaction of BMGs with diamond tools at different conditions has produced fundamental information on the mechanism in diamond turning of BMGs. The characteristics of the chip formation and finish surface revealed the deformation mechanism in diamond turning. Oxidation and crystallization have been found to occur under specific cutting parameters. Research on the mechanism can be utilized to optimize the parameters for optical level finish surface quality. Some optical applications, such as fabrication of microlens array or microchannel on BMGs molds, are getting popular in glass molding. The diamond turning has become a necessity tool that is capable of processing BMGs for complicated freeform surfaces with high profile accuracy and fine surface integrity. With further development of BMGs, it is necessary to continue the investigation on efficient and economical microstructure machining of BMGs by shortening time and extending tool lifespan, which could be further applied in industry. Moreover, it is also important to identify appropriate parameters that result in profile accuracy and fine surface integrity, in particularly without crystallization and oxidation.

Laser processing The laser processing of BMGs is still a relatively young research field. Even though such studies are comparatively scarce, the nanosecond pulsed laser showed great promise to form sophisticated hierarchical geometries. Up to now, by observing the residual ripple patterns around the crater induced by laser irradiation, the material removal mechanism was uncovered gradually, which was related to local material melt, vaporization, and solidification with instable conditions. The characteristics of the irradiated surface were no longer the same with non-irradiated surfaces on hardness and atomic structures. However, our understanding of the interaction between the BMG and nanosecond pulsed laser was far from complete. On the one hand, the cycle for each nanosecond laser pulse was really short within very tiny local area. No appropriate in situ instrument can catch up the phenomenon during this process. On the other hand, an accurate simulation is not a minor challenge, and developing a complete temperature field model during laser irradiation is a complex task when

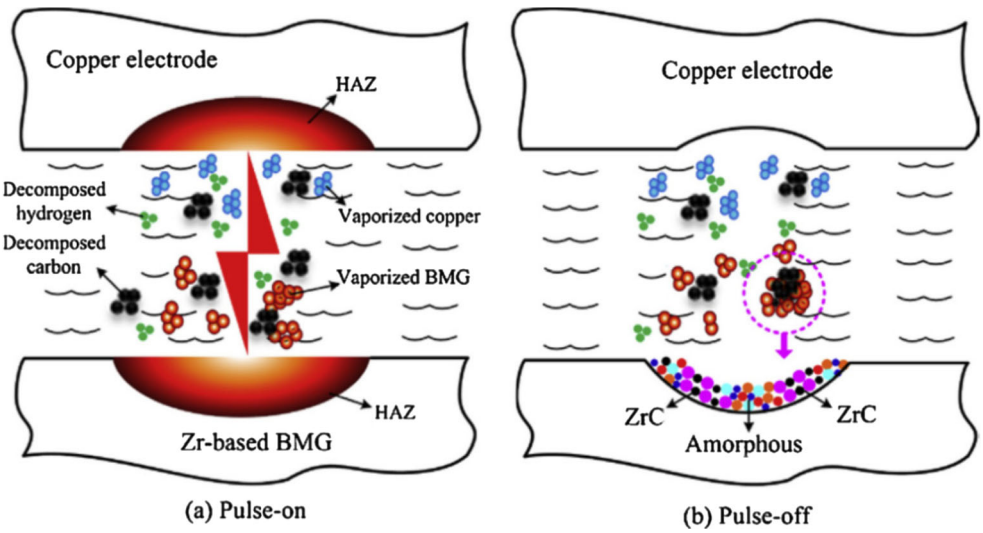

Fig. 32 Schematic diagram illustrating the formation of ZrC phase in micro-EDM [92]

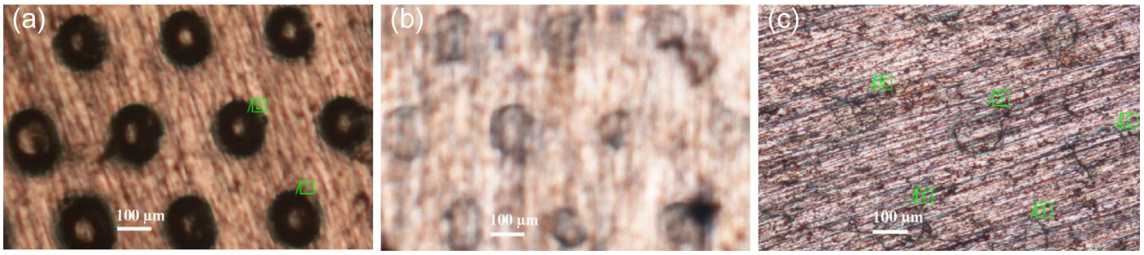

Fig. 33 Microlens array on the mold is used for hot embossing onto $Mg_{58}Cu_{31}Y_{11}$ BMGs alloy at 150 °C under pressure of **a** 10 MPa for 10 min; **b** 5 MPa for 10 min; and **c** 1 MPa for 10 min [94]

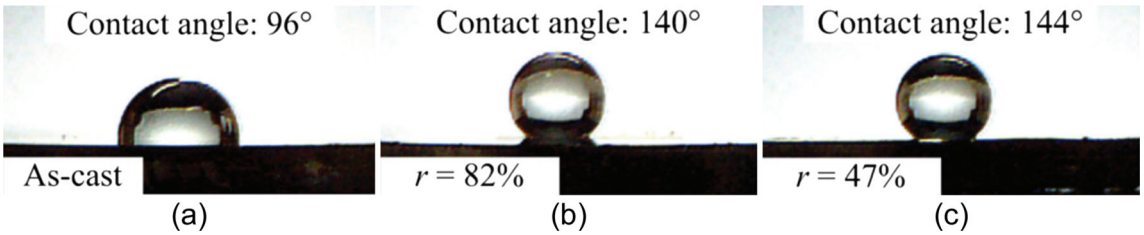

Fig. 34 Contact angle of as-cast (**a**) and laser patterned BMG surface (*r* is the pulse overlap rate) [86]

considering vaporization, plasma effects as well as chemical composition changes in the material. Thus, as the development of lasers continues and the number of available BMGs increases, comprehensive research should be continued on the mechanism investigation by introducing more in situ analysis methods. In addition, it is also necessary to continue the study of using lasers to irradiate at a micro scale with appropriate parameters that result in efficient micro machining of a variety of BMGs and carefully controlled removal of material without damaging the materials themselves.

Micro-EDM Material removal on the BMG surfaces using micro-EDM showed promise on hierarchical structures fabrication with great flexibility. However, as a novel kind of manufacturing method in BMG machining, the research results presented in current studies indicated that it is difficult to achieve truly amorphous structure together with fine surface integrity. This may greatly restrict its wide usage and applications in industry and civil life. Thus, there is an avenue for refinement through further investigations such as developing hybrid machining method.

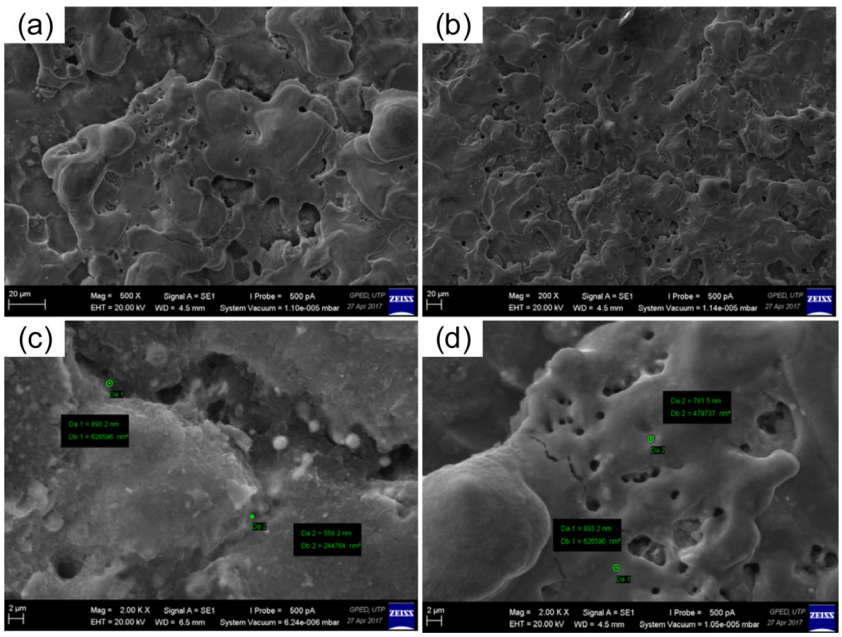

Fig. 35 The EDMed surface of BMGs at different experimental conditions [96]

Acknowledgements The authors would like to thank all colleagues and collaborators who have contributed to various aspects of the research reported in this work.

Funding information This work was financially supported by the National Natural Science Foundation of China (Grant No. 51705197), Young Elite Scientists Sponsorship Program by CAST(YESS) (Grant No. 2017QNRC001), and the Fundamental Research Funds for the Central Universities.

References

1. Schroers J (2010) Processing of bulk metallic glass. Adv Mater 22(14):1566–1597
2. Jun WK, Willens RH, Duwez P (1960) Non-crystalline structure in solidified gold–silicon alloys. Nature 187:869
3. Chen HS, Turnbull D (1969) Formation, stability and structure of palladium-silicon based alloy glasses. Acta Metall 17(8):1021–1031
4. Li N, Chen W, Liu L (2016) Thermoplastic micro-forming of bulk metallic glasses: a review. JOM 68(4):1246–1261
5. Peker A, Johnson WL (1993) A highly processable metallic glass: $Zr_{41.2}Ti_{13.8}Cu_{12.5}Ni_{10.0}Be_{22.5}$. Appl Phys Lett 63(17):2342–2344
6. Lin XH, Johnson WL (1995) Formation of Ti-Zr-Cu-Ni bulk metallic glasses. J Appl Phys 78(11):6514–6519
7. Hays CC, Schroers J, Geyer U, Bossuyt S, Stein N, Johnson WL (2000) Glass forming ability in the Zr-Nb-Ni-Cu-Al bulk metallic glasses. J Metastable Nanocrystalline Mater 8:103–108
8. Inoue A, Zhang T, Masumoto T (1990) Zr-Al-Ni amorphous alloys with high glass transition temperature and significant supercooled liquid region. Mater Trans JIM 31(3):177–183
9. Inoue A, Nishiyama N, Amiya K, Zhang T, Masumoto T (1994) Ti-based amorphous alloys with a wide supercooled liquid region. Mater Lett 19(14–15):131–135
10. Kim YC, Kim WT, Kim DH (2004) A development of Ti-based bulk metallic glass. Mater Sci Eng A 375–377:127–135
11. Inoue A, Zhang W, Zhang T, Kurosaka K (2001) High-strength Cu-based bulk glassy alloys in Cu-Zr-Ti and Cu-Hf-Ti ternary systems. Acta Mater 49(14):2645–2652
12. Dai C-L, Guo H, Shen Y, Li Y, Ma E, Xu J (2006) A new centimeter-diameter Cu-based bulk metallic glass. Scr Mater 54(7):1403–1408
13. Ponnambalam V, Poon SJ, Shiflet GJ (2004) Fe-based bulk metallic glasses with diameter thickness larger than one centimeter. J Mater Res 19(5):1320–1323
14. Lu ZP, Liu CT, Thompson JR, Porter WD (2004) Structural amorphous steels. Phys Rev Lett 92:245503
15. Ponnambalam V, Poon SJ, Shiflet GJ, Keppens VM, Taylor R, Petculescu G (2003) Synthesis of iron-based bulk metallic glasses as nonferromagnetic amorphous steel alloys. Appl Phys Lett 83(6):1131–1133
16. Ma H, Xu J, Ma E (2003) Mg-based bulk metallic glass composites with plasticity and high strength. Appl Phys Lett 83(14):2793–2795
17. Inoue A, Kato A, Zhang T, Kim SG, Masumoto T (1991) Mg-Cu-Y amorphous alloys with high mechanical strengths produced by a metallic mold casting method. Mater Trans JIM 32(7):609–616
18. Inoue A, Ohtera K, Kita K, Masumoto T (1988) New amorphous Mg-Ce-Ni alloys with high strength and good ductility. Jpn J Appl Phys 27:L2248–L2251
19. Choi-Yim H, Xu D, Johnson WL (2003) Ni-based bulk metallic glass formation in the Ni-Nb-Sn and Ni-Nb-Sn-X (X=B,Fe,Cu) alloy systems. Appl Phys Lett 82(7):1030–1032
20. Yi S, Park TG, Kim DH (2000) Ni–based bulk amorphous alloys in the Ni-Ti-Zr-(Si, Sn) system. J Mater Res 15(11):2425–2430
21. Lu I-R, Wilde G, Görler GP, Willnecker R (1999) Thermodynamic properties of Pd-based glass-forming alloys. J Non-Cryst Solids 250–252:577–581
22. Kui HW (1993) Formation of bulk $Pd_{40}Ni_{40}P_{20}$ glass. Appl Phys Lett 62(11):1224–1226
23. Nishiyama N, Inoue A (1996) Glass-forming ability of bulk $Pd_{40}Ni_{10}Cu_{30}P_{20}$ alloy. Mater Trans JIM 37:1531–1539
24. Chen M (2011) A brief overview of bulk metallic glasses. NPG Asia Mater 3:82–90
25. Huang Y, He F, Fan H, Shen J (2012) Ductile Ti-based metallic glass spheres. Scr Mater 67(7–8):661–664
26. Inoue A, Takeuchi A (2011) Recent development and application products of bulk glassy alloys. Acta Mater 59(6):2243–2267
27. Williams E, Lavery N (2017) Laser processing of bulk metallic glass: a review. J Mater Process Technol 247:73–91
28. Argon AS (1979) Plastic deformation in metallic glasses. Acta Metall 27:47–58
29. Duan G, Wiest A, Lind ML, Li J, Rhim WK, Johnson WL (2007) Bulk metallic glass with benchmark thermoplastic processability. Adv Mater 19(23):4272–4275
30. Zhu Z, Zhou X, Liu Q, Lin JQ, Zhao SX (2012) Fabrication of micro-structured surfaces on bulk metallic glasses based on fast tool servo assisted diamond turning. Sci Adv Mater 4(9):906–911
31. Yu DP, Gan SW, Wong YS, Hong GS, Rahman M, Yao J (2012) Optimized tool path generation for fast tool servo diamond turning of micro-structured surfaces. Int J Adv Manuf Technol 63(9–12):1137–1152
32. Zhang XD, Fang FZ, Wu QQ, Liu XL, Gao HM (2013) Coordinate transformation machining of off-axis aspheric mirrors. Int J Adv Manuf Technol 67(9–12):2217–2224
33. Tian F, Yin Z, Li S (2016) A novel long range fast tool servo for diamond turning. Int J Adv Manuf Technol 86(5–8):1227–1234
34. Sosnicki O, Pages A, Pacheco C, Maillard T (2010) Servo piezo tool SPT400MML for the fast and precise machining of free forms. Int J Adv Manuf Technol 47(9–12):903–910
35. Zhu L, Li Z, Fang F, Huang SY, Zhang XD (2018) Review on fast tool servo machining of optical freeform surfaces. Int J Adv Manuf Technol 95(5–8):2071–2092
36. Zhu Z, To S (2015) Adaptive tool servo diamond turning for enhancing machining efficiency and surface quality of freeform optics. Opt Express 23(16):20234–20248
37. Zhu Z, To S, Zhang S (2015) Theoretical and experimental investigation on the novel end-fly-cutting-servo diamond machining of hierarchical micro-nanostructures. Int J Mach Tools Manuf 94:15–25
38. Zhu Z, To S, Zhang S (2015) Large-scale fabrication of micro-lens array by novel end-fly-cutting-servo diamond machining. Opt Express 23(16):20593–20604
39. Guo P, Lu Y, Ehmann KF, Cao J (2014) Generation of hierarchical micro-structures for anisotropic wetting by elliptical vibration cutting. CIRP Ann 63(1):553–556
40. Bakkal M, Shih AJ, McSpadden SB, Liu CT, Scattergood RO (2005) Light emission, chip morphology, and burr formation in drilling the bulk metallic glass. Int J Mach Tools Manuf 45(7–8):741–752
41. Bakkal M, Shih AJ, Scattergood RO, Liu CT (2004) Machining of a Zr-Ti-Al-Cu-Ni metallic glass. Scr Mater 50(5):583–588
42. Bakkal M, Shih AJ, Scattergood RO (2004) Chip formation, cutting forces, and tool wear in turning of Zr-based bulk metallic glass. Int J Mach Tools Manuf 44(9):915–925

43. Han DX, Wang G, Li J, Chan KC, To S, Wu FF, Gao YL, Zhai QJ (2015) Cutting characteristics of Zr-based bulk metallic glass. J Mater Sci Technol 31(2):153–158
44. Sugioka K, Meunier M, Piqué A (2010) Laser precision microfabrication. Springer-Verlag, Berlin Heidelberg
45. Knowles MRH, Rutterford G, Karnakis D, Ferguson A (2007) Micro-machining of metals, ceramics and polymers using nanosecond lasers. Int J Adv Manuf Technol 33(1–2):95–102
46. Dhara SK, Kuar AS, Mitra S (2008) An artificial neural network approach on parametric optimization of laser micro-machining of die-steel. Int J Adv Manuf Technol 39(1–2):39–46
47. Mathew MM, Bathe RN, Padmanabham G, Padmanaban R, Thirumalini S (2017) A study on the micromachining of molybdenum using nanosecond and femtosecond lasers. Int J Adv Manuf Technol. https://doi.org/10.1007/s00170-017-1454-z
48. Pecholt B, Vendan M, Dong Y, Molian P (2008) Ultrafast laser micromachining of 3C-SiC thin films for MEMS device fabrication. Int J Adv Manuf Technol 39(3–4):239–250
49. Quintana I, Dobrev T, Aranzabe A, Lalev G, Dimov S (2009) Investigation of amorphous and crystalline Ni alloys response to machining with micro-second and pico-second lasers. Appl Surf Sci 255(13–14):6641–6646
50. Quintana I, Dobrev T, Aranzabe A, Lalev G (2010) Laser micromachining of metallic glasses: investigation of the material response to machining with micro-second and pico-second lasers. International Society for Optics and Photonics, Bellingham, p 75840Y
51. Vella PC, Dimov SS, Brousseau E, Whiteside BR (2015) A new process chain for producing bulk metallic glass replication masters with micro- and nano-scale features. Int J Adv Manuf Technol 76(1–4):523–543
52. Richard J, Demellayer R (2013) Micro-EDM-milling development of new machining technology for micro-machining. Procedia CIRP 6:292–296
53. Li H, Wang Z, Wang Y, Liu HZ, Bai YF (2017) Micro-EDM drilling of ZrB_2-SiC-graphite composite using micro sheet-cylinder tool electrode. Int J Adv Manuf Technol 92(5–8):2033–2041
54. D'Urso G, Giardini C, Quarto M (2018) Characterization of surfaces obtained by micro-EDM milling on steel and ceramic components. Int J Adv Manuf Technol 97(5–8):2077–2085
55. Hsieh SF, Chen SL, Lin MH, Ou SF (2013) Crystallization and carbonization of an electrical discharge machined Zr-based bulk metallic glass alloy. J Mater Res 28(22):3177–3184
56. Axinte E (2012) Metallic glasses from "alchemy" to pure science: present and future of design, processing and applications of glassy metals. Mater Des 35:518–556
57. Lu ZP, Liu CT (2004) Role of minor alloying additions in formation of bulk metallic glasses: a review. J Mater Sci 39(12):3965–3974
58. Zhang SJ, To S, Wang SJ, Zhu ZW (2015) A review of surface roughness generation in ultra-precision machining. Int J Mach Tools Manuf 91:76–95
59. Fujita K, Morishita Y, Nishiyama N, Kimura H, Inoue A (2005) Cutting characteristics of bulk metallic glass. Mater Trans 46(12): 2856–2863
60. Bakkal M, Nakş[idot]ler V (2009) Cutting mechanics of bulk metallic glass materials on meso-end milling. Mater Manuf Process 24(12):1249–1255
61. Komanduri R, Brown RH (1981) On the mechanics of chip segmentation in machining. J Eng Ind 103(1):33–51
62. Sheikh-Ahmad J, Bailey JA (1997) Flow instability in the orthogonal machining of CP titanium. J Manuf Sci Eng 119(3):307–313
63. López de lacalle LN, Pérez J, Llorente JI, Sánchez JA (2000) Advanced cutting conditions for the milling of aeronautical alloys. J Mater Process Technol 100:1–3):1–11
64. Shivpuri R, Hua J, Mittal P, Srivastava AK, Lahoti GD (2002) Microstructure-mechanics interactions in modeling chip segmentation during titanium machining. CIRP Ann 51(1):71–74
65. Choudhury IA, El-Baradie MA (1998) Machinability of nickel-base super alloys: a general review. J Mater Process Technol 77(1–3): 278–284
66. Komanduri R, Schroeder TA (1986) On shear instability in machining a nickel-iron base superalloy. J Eng Ind 108:93–100
67. Jiang MQ, Dai LH (2009) Formation mechanism of lamellar chips during machining of bulk metallic glass. Acta Mater 57(9):2730–2738
68. Bakkal M, Liu CT, Watkins TR, Scattergood RO, Shih AJ (2004) Oxidation and crystallization of Zr-based bulk metallic glass due to machining. Intermetallics 12(2):195–204
69. Williams E, Brousseau EB (2016) Nanosecond laser processing of $Zr_{41.2}Ti_{13.8}Cu_{12.5}Ni_{10}Be_{22.5}$ with single pulses. J Mater Process Technol 232:34–42
70. Wang HS, Wu JY, Liu YT (2016) Effect of the volume fraction of the ex-situ reinforced Ta additions on the microstructure and properties of laser-welded Zr-based bulk metallic glass composites. Intermetallics 68:87–94
71. Yamasaki M, Kagao S, Kawamura Y, Yoshimura K (2004) Thermal diffusivity and conductivity of supercooled liquid in $Zr_{41}Ti_{14}Cu_{12}Ni_{10}Be_{23}$ metallic glass. Appl Phys Lett 84(23): 4653–4655
72. Ma F, Yang J, Zhu XN, Liang CY, Wang HS (2010) Femtosecond laser-induced concentric ring microstructures on Zr-based metallic glass. Appl Surf Sci 256(11):3653–3660
73. Yang J, Zhao Y, Zhang N, Liang YM, Wang MW (2007) Ablation of metallic targets by high-intensity ultrashort laser pulses. Phys Rev B 76(16):165430
74. Yang Y, Yang J, Liang C, Wang HS, Zhu XN, Kuang DF, Yang Y (2008) Sub-wavelength surface structuring of NiTi alloy by femtosecond laser pulses. Appl Phys A Mater Sci Process 92(3):635–642
75. Borowiec A, Haugen HK (2003) Subwavelength ripple formation on the surfaces of compound semiconductors irradiated with femtosecond laser pulses. Appl Phys Lett 82(25):4462–4464
76. Wang J, Guo C (2005) Ultrafast dynamics of femtosecond laser-induced periodic surface pattern formation on metals. Appl Phys Lett 87(25):251914
77. Liu Y, Jiang MQ, Yang GW, Guan YJ, Dai LH (2011) Surface rippling on bulk metallic glass under nanosecond pulse laser ablation. Appl Phys Lett 99(19):191902
78. Ang LK, Lau YY, Gilgenbach RM, Spindler HL, Lash JS, Kovaleski SD (1998) Surface instability of multipulse laser ablation on a metallic target. J Appl Phys 83(8):4466–4471
79. Fan GJ, Liao HH, Choo H, Liaw PK, Mara N, Sergueeva AV, Mukherjee AK, Lavernia EJ (2007) Fracture of a commercial $Zr_{41.2}Ti_{13.8}Cu_{12.5}Ni_{10.0}Be_{22.5}$ bulk-metallic glass. Metall Mater Trans A 38(9):2001–2005
80. Wu B (2008) High-intensity nanosecond-pulsed laser-induced plasma in air, water, and vacuum: a comparative study of the early-stage evolution using a physics-based predictive model. Appl Phys Lett 93(10):101104
81. Busch R, Bakke E, Johnson WL (1998) Viscosity of the supercooled liquid and relaxation at the glass transition of the $Zr_{46.75}Ti_{8.25}Cu_{7.5}Ni_{10}Be_{27.5}$ bulk metallic glass forming alloy. Acta Mater 46(13):4725–4732
82. Liu Y, Jiang MQ, Yang GW, Chen JH, Guan YJ, Dai LH (2012) Saffman–Taylor fingering in nanosecond pulse laser ablating bulk metallic glass in water. Intermetallics 31:325–329
83. Jiang MQ, Wei YP, Wilde G, Dai LH (2015) Explosive boiling of a metallic glass superheated by nanosecond pulse laser ablation. Appl Phys Lett 106(2):021904

84. Huang H, Jun N, Jiang M, Ryoko M, Yan JW (2016) Nanosecond pulsed laser irradiation induced hierarchical micro/nanostructures on Zr-based metallic glass substrate. Mater Des 109:153–161
85. Huang H, Noguchi J, Yan J (2016) Shield gas induced cracks during nanosecond-pulsed laser irradiation of Zr-based metallic glass. Appl Phys A Mater Sci Process 122:881
86. Huang H, Yan J (2017) Surface patterning of Zr-based metallic glass by laser irradiation induced selective thermoplastic extrusion in nitrogen gas. J Micromech Microeng 27:075007
87. Yan J, Watanabe K, Aoyama T (2014) Micro-electrical discharge machining of polycrystalline diamond using rotary cupronickel electrode. CIRP Ann 63(1):209–212
88. Prakash V, Kumar P, Singh PK, Hussain M, Das AK, Chattopadhyaya S (2017) Micro-electrical discharge machining of difficult-to-machine materials: a review. Proc Inst Mech Eng Part B J Eng Manuf. https://doi.org/10.1177/0954405417718591
89. Hourmand M, Sarhan AAD, Sayuti M (2017) Micro-electrode fabrication processes for micro-EDM drilling and milling: a state-of-the-art review. Int J Adv Manuf Technol 91(1–4):1023–1056
90. Yeo SH, Tan PC, Aligiri E, Tor SB, Loh NH (2009) Processing of zirconium-based bulk metallic glass (BMG) using micro electrical discharge machining (micro-EDM). Mater Manuf Process 24(12): 1242–1248
91. Chen XH, Zhang XC, Zhang Y, Chen GL (2008) Fabrication and characterization of metallic glasses with a specific microstructure for micro-electro-mechanical system applications. J Non-Cryst Solids 354(28):3308–3316
92. Huang H, Yan J (2015) On the surface characteristics of a Zr-based bulk metallic glass processed by microelectrical discharge machining. Appl Surf Sci 355:1306–1315
93. Huang H, Yan J (2016) Microstructural changes of Zr-based metallic glass during micro-electrical discharge machining and grinding by a sintered diamond tool. J Alloys Compd 688:14–21
94. Pan CT, Wu TT, Liu YT, Yamagata Y, Huang JC (2009) Fabrication of aspheric surface using ultraprecision cutting and BMG molding. J Mater Process Technol 209(11):5014–5023
95. Li HF, Zheng YF (2016) Recent advances in bulk metallic glasses for biomedical applications. Acta Biomater 36:1–20
96. Aliyu AAA, Abdul-Rani AM, Ginta TL, Prakash C, Axinte E, Fua-Nizan R (2017) Investigation of nanoporosities fabricated on metallic glass surface by hydroxyapatite mixed EDM for orthopedic application. Malays J Fundam Appl Sci 13:523–528